



UNIVERSITY OF LEEDS

This is a repository copy of *Devonian paleoclimate and its drivers: A reassessment based on a new conodont  $\delta^{18}O$  record from South China.*

White Rose Research Online URL for this paper:

<https://eprints.whiterose.ac.uk/179081/>

Version: Accepted Version

---

**Article:**

Chen, B, Ma, X, Mills, BJW [orcid.org/0000-0002-9141-0931](https://orcid.org/0000-0002-9141-0931) et al. (6 more authors) (2021) Devonian paleoclimate and its drivers: A reassessment based on a new conodont  $\delta^{18}O$  record from South China. *Earth-Science Reviews*, 222. 103814. ISSN 0012-8252

<https://doi.org/10.1016/j.earscirev.2021.103814>

---

© 2021 Elsevier B.V. This is an author produced version of a paper published in *Earth-Science Reviews*. Uploaded in accordance with the publisher's self-archiving policy. This manuscript version is made available under the Creative Commons CC-BY-NC-ND 4.0 license <http://creativecommons.org/licenses/by-nc-nd/4.0/>.

**Reuse**

This article is distributed under the terms of the Creative Commons Attribution-NonCommercial-NoDerivs (CC BY-NC-ND) licence. This licence only allows you to download this work and share it with others as long as you credit the authors, but you can't change the article in any way or use it commercially. More information and the full terms of the licence here: <https://creativecommons.org/licenses/>

**Takedown**

If you consider content in White Rose Research Online to be in breach of UK law, please notify us by emailing [eprints@whiterose.ac.uk](mailto:eprints@whiterose.ac.uk) including the URL of the record and the reason for the withdrawal request.



[eprints@whiterose.ac.uk](mailto:eprints@whiterose.ac.uk)  
<https://eprints.whiterose.ac.uk/>

1 Devonian paleoclimate and its drivers: A reassessment based on a new  
2 conodont  $\delta^{18}\text{O}$  record from South China

3 Bo Chen <sup>a\*</sup>, Xueping Ma <sup>b</sup>, Benjamin J.W. Mills<sup>c</sup>, Wenkun Qie<sup>a</sup>, Michael M. Joachimski  
4 <sup>d</sup>, Shuzhong Shen <sup>e</sup>, Chengyuan Wang <sup>a</sup>, Honghe Xu <sup>a</sup>, Xiangdong Wang <sup>e</sup>

5  
6 <sup>a</sup> State Key Laboratory of Palaeobiology and Stratigraphy and Center for Excellence in  
7 Life and Paleoenvironment, Nanjing Institute of Geology and Palaeontology, Chinese  
8 Academy of Sciences, Nanjing, 210008, China

9 <sup>b</sup> School of Earth and Space Sciences, Peking University, Beijing 100871, China

10 <sup>c</sup> School of Earth and Environment, University of Leeds, Leeds, LS2 9JT, UK

11 <sup>d</sup> GeoZentrum Nordbayern, Friedrich-Alexander-Universität Erlangen-Nürnberg, 91054  
12 Erlangen, Germany

13 <sup>e</sup> State Key Laboratory for Mineral Deposits Research, School of Earth Sciences and  
14 Engineering and Frontiers Science Center for Critical Earth Material Cycling, Nanjing  
15 University, 210093, Nanjing, China

16  
17 \* [chenbo@nigpas.ac.cn](mailto:chenbo@nigpas.ac.cn)

18  
19 **Abstract**

20 **A new Devonian oxygen isotope record based on 180 measurements of**  
21 **conodont apatite is reported from South China. The comparison with published**  
22 **Devonian  $\delta^{18}\text{O}_{\text{apatite}}$  data shows a considerable offset between records from**  
23 **different paleocontinents. This difference can be interpreted by regional variations**  
24 **in salinity, with the epicontinental seas having a distinctly lower salinity and**  
25  **$\delta^{18}\text{O}_{\text{seawater}}$  than the open ocean due to the influence of fresh-water runoff. Our**  
26 **findings suggest that the oxygen isotope record from open ocean settings is the**  
27 **preferred archive for reconstructing the history of ocean temperature and/or ice**  
28 **volume over the Phanerozoic**

29 **Despite regional differences, the South China and European records show**  
30 **similar long-term trends characterized by a pronounced cooling during the**  
31 **Pragian to Eifelian followed by significant warming over the Eifelian/Givetian to**  
32 **Frasnian, and a further cooling starting in the Famennian, accelerating in the**  
33 **earliest Carboniferous. The Early Devonian cooling coincided with early vascular**  
34 **plant root–soil interactions and a significant diversity increase in both spores and**

35 megaplant fossils, suggesting that the rise of rooted vascular plants may have  
36 played a key role in triggering climate cooling. Subsequent climatic warming over  
37 the Middle to Late Devonian transition may have been linked to metamorphic CO<sub>2</sub>  
38 input from the Acadian Orogeny, while Famennian cooling occurred in a context  
39 of exposure and weathering of basalts and ophiolites and coincided with the advent  
40 of seed plants. We conclude that climate changes during the Devonian were likely  
41 driven by a combination of plant evolutionary advances and changes in tectonics.

42 We further test these interpretations by running the COPSE (Carbon, Oxygen,  
43 Phosphorus, Sulphur and Evolution) biogeochemical model. The model prediction  
44 is capable of reproducing the *p*CO<sub>2</sub> record under these scenarios, although the  
45 model is not capable of reproducing the degree of temperature variation, likely  
46 due to its simplicity.

47 Key words: Paleotemperatures; Vascular vegetation; Acadian Orogeny; Volcanism;  
48 Regional δ<sup>18</sup>O difference

49

## 50 1 Introduction

51 The Devonian period was characterized by the radiation of vascular plants. The  
52 colonization of the terrestrial landscape by rooted vascular plants is considered to have  
53 been a key factor in driving changes in Devonian climate (Berner, 2003). The so-called  
54 “Devonian plant hypothesis” (Algeo et al., 1995; 2001) proposed that the appearance  
55 of trees with deep root systems and the establishment of forests in the Middle Devonian  
56 (Meyer-Berthaud et al., 2010; Stein et al., 2012; Giesen and Berry, 2013) may have  
57 accelerated silicate weathering and/or organic carbon burial (Sandberg et al. 1988;  
58 Joachimski et al., 2002; Joachimski and Buggisch, 2002), resulting in multiple oceanic  
59 anoxic events (Algeo et al., 2001), lower atmospheric CO<sub>2</sub> levels (Berner, 2003; Taylor  
60 et al. 2009), and global climatic cooling as documented in a brief glaciation in the Late  
61 Devonian-Carboniferous boundary (Caputo et al., 2008). However, the climatic  
62 consequences of Devonian plant expansion have not been well evaluated in the context  
63 of reliable paleoclimatic reconstructions. Atmospheric *p*CO<sub>2</sub> reconstructions are sparse  
64 for the Devonian (Royer et al., 2014; Foster et al., 2017), whereas modelling generally

65 predicts a major drop in  $p\text{CO}_2$  in the late Early Devonian (ca. 400 Ma late Emsian;  
66 [Lenton et al., 2016, 2018](#)). Reconstructions of seawater temperatures based on oxygen  
67 isotope ratios measured on marine calcitic or phosphatic fossils indicate long-term  
68 cooling through most of the Devonian with an interruption by a short but significant  
69 warming interval around the Middle to Late Devonian transition (Givetian to Frasnian)  
70 ([van Geldern et al, 2006; Joachimski et al., 2009](#)) which - according to the “Devonian  
71 plant hypothesis” ([Algeo et al., 2001](#)) - should be represented by significant climatic  
72 cooling. This detailed climate history points to a complex relationship between vascular  
73 plant colonization and Devonian climate. For example, in addition to plant evolution,  
74 the Devonian Period is characterized by multiple orogenies ([Stewart and Ague, 2018](#))  
75 and LIP (large igneous province) volcanic episodes especially in the Late Devonian  
76 ([Ernst et al, 2020; Racki, 2020](#)). These geological processes could have exerted a  
77 significant influence on Devonian climate, but their effects have not been systematically  
78 evaluated.

79 In this contribution, we provide a new Devonian conodont apatite oxygen isotope  
80 record measured on samples from the South China Craton. The new data confirm the  
81 major oxygen isotope shifts demonstrated in previous studies in Europe, North America  
82 and Australia ([Joachimski et al., 2004; 2009](#)), thus excluding local climate conditions  
83 (e.g., evaporation/precipitation ratio) as an important driver of the observed secular  
84 variations. We therefore consider the Devonian oxygen isotope records to principally  
85 reflect global climatic changes and interpret the significant changes in the context of  
86 plant cover expansion, volcanism and orogenic activities. We test these interpretations  
87 by using the COPSE biogeochemical model.

88

## 89 **2. Geological setting**

90 The study sections are located in the Guangxi Zhuang Autonomous Region, as well  
91 as in the Guizhou and Yunnan provinces in southwest China, where Devonian strata  
92 are well exposed and intensively studied. Paleogeographically, these sections were all  
93 located on the Yangtze Platform which, during the Devonian, was situated in low  
94 latitudes in the eastern Tethyan Ocean ([Fig. 1](#)). Except for the Qinfang Trough in

95 southern Guangxi, the study area was uplifted during the Late Silurian as a consequence  
96 of the Guangxi (Caledonian) Orogeny. Marine sedimentation started again in the  
97 earliest Devonian in the areas north of the Qinfang Trough (Wu et al., 1987; Liu et al.,  
98 1993; Chen et al., 2002, Chen et al., 2014) (Fig. 1 b, c) and progressively expanded  
99 northwards during the Middle to Late Devonian. This transgression is well recorded  
100 across Guangxi and adjacent areas, with Lochkovian deposits dominated by terrigenous  
101 siliciclastic followed by Pragian and Emsian siliciclastics interbedded with carbonates  
102 and Middle to Late Devonian carbonates.

103 Pragian conodonts were collected from the Dashatian section situated in Nanning  
104 City (Fig. 1). The section is characterized by siltstones and mudstones alternating with  
105 few carbonate beds. The conodont assemblage identified in this section includes  
106 *Eognathodus irregularis*, *E. nagaolingensis*, *E. sulcatus* mu morph, *Masaraella*  
107 *pandora* indicating an early Pragian age (Wang et al., 2016). Emsian to Givetian  
108 conodonts were collected mainly from the Changputang, Sihongshan, Nayi as well as  
109 Caiziyan sections. The Changputang section is situated at Wenshan in Southeastern  
110 Yunnan province (Fig. 1) and is characterized by alternating deep-water siliceous rocks  
111 or cherty limestones and shales with shallow water bioclastic and micritic limestones  
112 (Jin et al., 2005), indicating significant relative sea level fluctuations. The Sihongshan  
113 section is located at Debao County, in southwestern Guangxi Zhuang Autonomous  
114 Region. The section is composed of pelagic and dolomitic limestones alternating with  
115 few siliceous horizons. A nearly complete conodont sequence from the Early Devonian  
116 *Polygnathus excavatus* Zone (Emsian) to Late Devonian *Palmatolepis crepida* Zone  
117 (Famennian) was identified in this section (Ziegler and Wang, 1985). The Caiziyan  
118 section is located approximately 30 km northeast of Guilin city in Guangxi. The  
119 conodont biostratigraphy of the exposed Givetian–Frasnian boundary interval is well  
120 studied in this section, with 10 standard conodont zones being identified (Li et al., 2009).

121 Frasnian-Famennian conodont samples were collected from the Dongcun and  
122 Huohua sections. The Dongcun section is located at about 20 km northwest of Yangsuo  
123 County in Guangxi and is mainly composed of limestones with few inter-bedded  
124 dolomites, representing marginal platform and slope facies with abundant pelagic

125 faunas, especially conodonts (Wang, 1994). Conodont zones range from the Early  
126 Frasnian *Polygnathus transitans* to the early Famennian *P. crepida* Zone (Wang, 1994;  
127 Wang and Ziegler, 2002) with the Frasnian/Famennian boundary precisely identified in  
128 the upper part of the section (Wang and Ziegler, 2002). The Huohua Section is situated  
129 in Ziyun County in south Guizhou (Fig. 1) where carbonates yielding abundant  
130 conodonts have been deposited in marginal platform and slope settings during the  
131 Frasnian to the earliest Carboniferous. The stratigraphic range of the sampled intervals  
132 in the study sections is shown in Fig. 2.

133

### 134 3. Material and methods

135

#### 136 3.1 Oxygen isotope analyses of conodont apatite

137 Conodonts were extracted by dissolving carbonate rocks in 10% acetic acid.  
138 Residues were separated using heavy liquid fractionation (lithium-polytungstate).  
139 Conodont elements were picked from the heavy fraction under a binocular microscope.  
140 0.5 to 1.0 mg conodont apatite was weighed into a small polyethylene beaker, and 5 ml  
141 2 M HNO<sub>3</sub> was added to completely dissolve conodont apatite. The clear solution was  
142 pipetted to a new beaker and chemically converted to Ag<sub>3</sub>PO<sub>4</sub> following the method  
143 described by Joachimski et al. (2009). The obtained Ag<sub>3</sub>PO<sub>4</sub> crystals were ultrasonically  
144 washed 5 times with distilled water, dried at 60 °C for 1 hour and ground to fine powder  
145 using an agate mortar. 0.2 to 0.3 mg Ag<sub>3</sub>PO<sub>4</sub> powder was weighed into silver foil, which  
146 was transferred to the sample carousel of a TC-EA (high temperature elemental analyser)  
147 coupled online to a Thermo Fisher Delta Advanced IRMS. Sample and standard  
148 Ag<sub>3</sub>PO<sub>4</sub> samples were combusted at 1450 °C by TC-EA and the generated CO gas was  
149 transferred in a helium stream via a Conflo IV interface to the mass spectrometer. All  
150 oxygen isotope values are reported in ‰ relative to VSMOW. The average oxygen  
151 isotopic composition of NBS 120c standard was measured as 21.7‰ VSMOW.  
152 Accuracy was monitored by replicate analyses of NBS120c. Reproducibility was  
153 calculated based on triplicate sample and standard analyses and was generally < ±0.3‰  
154 (1 std. dev.).

155 Despite the oxygen isotopic composition of conodont apatite being relatively  
156 resistant to diagenetic alteration (Joachimski et al., 2009), a potential isotopic overprint  
157 by microbiological activity mediated by enzymes (Zazzo et al., 2004) or by diagenetic  
158 fluids at high temperatures (Puc at et al., 2004) is possible. Unfortunately, there is no  
159 robust method at present to identify post-depositional exchange of oxygen isotopes in  
160 biogenic apatite (Buggisch et al., 2008; Joachimski et al., 2009). For example, REE and  
161 trace element patterns as well as cathodoluminescence characteristics, as usually used  
162 for evaluating the preservation of brachiopod calcite (e.g. Garbelli et al., 2017), are  
163 demonstrated to be invalid in identifying exchange of oxygen in the phosphate ion of  
164 biogenic apatite (Buggisch et al., 2008; Joachimski et al., 2009). The conodont color  
165 alteration index (CAI) is a proxy for the maximum thermal overprint of sediments  
166 (Rejebian et al., 1987), with a high thermal overprint potentially causing  
167 recrystallisation (aggrading neomorphism) of conodont apatite (N oth, 1998). The  
168 varying CAI value is suspected as a potential reason for the symmetric  $\delta^{18}\text{O}_{\text{apatite}}$  values  
169 discrepancy between coeval late Permian sections in South China (Chen et al., 2016,  
170 Shen et al., 2019). However, several studies have found no major difference in oxygen  
171 isotope ratios from time-equivalent conodont samples with CAI values ranging from 1  
172 (corresponding to  $\sim 75^\circ\text{C}$ ) to 7 ( $>300^\circ\text{C}$ ) (Buggisch et al., 2008; Joachimski et al., 2009;  
173 Trotter et al., 2015), suggesting that intense heating does not necessarily result in  
174 oxygen isotope exchange in apatite phosphate. Similar  $\delta^{18}\text{O}_{\text{apatite}}$  values and/or trends  
175 in coeval sections are considered to document the preservation of primary  $\delta^{18}\text{O}$  signals  
176 (Joachimski et al., 2009; Huang et al., 2018).

177

178 In order to reconstruct long-term trends, the nonparametric locally weighted  
179 regression method ‘Locfit’ is utilized to calculate isotope trend lines (Loader, 1999).  
180 Locfit produces a smoothed curve retaining local minima and maxima and yields good  
181 results, even with unevenly spaced data points. All calculations were performed with  
182 the open source statistic software ‘R’ (version 3.3.1, Ihaka and Gentleman, 1996).

183

184 3.2 COPSE model

185 To explore drivers of Devonian climate change, we compare our dataset to the  
186 COPSE global biogeochemical model (Lenton et al., 2018). We plot the latest ‘baseline’  
187 model run from Tostevin and Mills (2020) and consider some basic alterations which  
188 may enable the model to better fit the data. COPSE considers the cycling of carbon,  
189 oxygen, phosphorus and sulfur over geological timescales. The model equations are  
190 described in full in Tostevin and Mills (2020).

191

## 192 **4. Results**

193 A total of 180 conodont apatite oxygen measurements spanning the Devonian were  
194 performed (Fig. 3A). An additional 103  $\delta^{18}\text{O}_{\text{apatite}}$  values of Frasnian-Famennian  
195 conodonts from South China reported by Huang et al. (2018) were used to construct a  
196  $\delta^{18}\text{O}_{\text{apatite}}$  curve for South China. The new data from South China show a  $\sim 2\%$  variance  
197 in  $\delta^{18}\text{O}$  apatite from the given time intervals, which is in the range by previous  
198 reconstructions (e.g. Joachimski et al., 2009; Chen et al., 2013; 2016). Mean values  
199 calculated using Locfit are around  $\sim 17\%$  during the Pragian followed by a pronounced  
200 rise to maximum value  $\sim 20.5\%$  in the Eifelian. Mean  $\delta^{18}\text{O}_{\text{apatite}}$  values decrease from  
201 approximately  $20.5\%$  to  $18\%$  in the Eifelian to early Frasnian and show a large  
202 variation with values between  $16\%$  and  $19\%$  across the Frasnian-Famennian  
203 boundary. Latest Famennian conodonts from South China yield  $\delta^{18}\text{O}_{\text{apatite}}$  values around  
204  $18\%$  at the Devonian-Carboniferous boundary (Fig. 3A), followed by a pronounced  
205 rise in  $\delta^{18}\text{O}_{\text{apatite}}$  in the earliest Carboniferous.

206

## 207 **5. Discussion**

### 208 **5.1 Comparison of $\delta^{18}\text{O}_{\text{apatite}}$ records from South China and other parts of the** 209 **World**

210 Comparable absolute  $\delta^{18}\text{O}_{\text{apatite}}$  values with systematic trends are observed in  
211 coeval Emsian samples from three different sections in South China (Shihongshan,  
212 Changputang and Nayi Sections, Fig. 3A). However, a systematic difference in  
213  $\delta^{18}\text{O}_{\text{apatite}}$  is observed for conodonts from two well-studied Frasnian-Famennian  
214 boundary sections (Huang et al. 2008), conodonts from the Yangdi section ( $17\text{-}19\%$ )



215 are on average 1‰ higher in  $\delta^{18}\text{O}_{\text{apatite}}$  compared to conodonts from the Dongcun  
216 section (16-18‰). Nevertheless, both records exhibit similar positive shifts at the  
217 Lower and Upper Kellwasser levels. Both sections were situated in close neighborhood  
218 in an inter-platform basin formed by rifting activity, representing a tropical open-  
219 marine setting without significant continental siliciclastic influx (Fig. 1C; [Chen et al.](#)  
220 [2001a, b, 2002](#)). Significant variations in seawater temperature and seawater  $\delta^{18}\text{O}$  (due  
221 to salinity changes) are unlikely, however there may have been a slight difference in  
222 depositional water depth. For example, the Yangdi section was deposited in a lower  
223 slope or basinal setting ([Huang et al., 2018](#); [Huang and Gong, 2016](#)). By contrast, the  
224 Dongcun section was deposited in a slightly shallower, possibly upper slope setting  
225 ([Wang and Ziegler, 2001](#); [Ma et al., 2008](#)). The systematic ~1‰ difference could be  
226 interpreted as reflecting differences in water depth, with conodonts from shallower  
227 waters (Dongcun section) recording 4 °C warmer temperatures than conodonts from the  
228 relative deeper water Yangdi section. However, this implies that *Palmatolepis*, the  
229 dominating conodont taxon measured in the two sections may have lived in slightly  
230 deeper parts of the water column, contradicting previous suggestions that *Palmatolepis*  
231 was a surface dweller ([Joachimski et al., 2009](#); [Huang et al., 2018](#)), but in line with the  
232 traditional conodont biofacies models (e.g. [Sandberg et al., 1988](#)) that considered  
233 *Palmatolepis* as a pelagic taxon which could have lived at variable water-depths.

234 The comparison of published  $\delta^{18}\text{O}_{\text{apatite}}$  records with the South China record shows  
235 that Pragian  $\delta^{18}\text{O}_{\text{apatite}}$  data from South China yield comparable values to those from  
236 Australia but lower  $\delta^{18}\text{O}_{\text{apatite}}$  values than those from Europe (Fig. 3 A, B), The late  
237 Emsian to Eifelian  $\delta^{18}\text{O}_{\text{apatite}}$  data from South China and Europe yield higher  $\delta^{18}\text{O}_{\text{apatite}}$   
238 values compared with those from Australia and USA (Fig. 4), with the regional  
239 differences in  $\delta^{18}\text{O}$  becoming less obvious during the Late Devonian and Early  
240 Carboniferous. The  $\delta^{18}\text{O}$  difference could be interpreted by regional effects such as  
241 salinity (e.g. via river discharge, upwelling, seasonal rainfall patterns). It is interesting  
242 that the discrepancy in  $\delta^{18}\text{O}_{\text{apatite}}$  appears to be dependent on the ocean basins, with  
243 China and Europe located in the Palaeotethys ocean yielding higher  $\delta^{18}\text{O}_{\text{apatite}}$  values,  
244 whereas western USA and Australia were situated in the Panthalassa ocean and have

245 lower  $\delta^{18}\text{O}_{\text{apatite}}$  values (Figs. 3 A, B). This observation may reflect freshwater runoff  
246 and thus lower salinities in the Panthalassa seas in southeastern Australia and the US  
247 Midcontinent (low  $\delta^{18}\text{O}_{\text{seawater}}$  value), while  $\delta^{18}\text{O}_{\text{apatite}}$  values from the shelf seas  
248 bordering the western (Europe) and eastern Palaeotethys (China) may represent an  
249 open-marine settings with higher salinities (high  $\delta^{18}\text{O}_{\text{seawater}}$  values). A similar pattern  
250 is observed in the Pennsylvanian North American Midcontinent Sea, which was an  
251 extensive tropical epicontinental sea within the Laurentian Craton (Heckel, 1977; Algeo  
252 and Heckel, 2008) with increased continental runoff resulting in an obvious offshore-  
253 onshore decrease in surface water  $\delta^{18}\text{O}$  (Joachimski and Lambert, 2015; Rosenau et al.,  
254 2014, Macarewich et al., 2021), and, resulting in considerably lower values ( $\sim 3\%$ ) of  
255 Pennsylvanian conodonts from the US Midcontinent compared to coeval conodonts  
256 from open ocean South China (Joachimski et al., 2006; Joachimski and Lambert, 2015;  
257 Chen et al., 2016). Using the  $\delta^{18}\text{O}$ -salinity relationship for modern tropical settings like  
258 the Gulf of Panama where a change of  $0.25\%$  in  $\delta^{18}\text{O}$  corresponds to a 1 psu salinity  
259 change (Tao et al., 2013), the observed  $\delta^{18}\text{O}$  difference of  $1.5\text{-}2.0\%$  between the  
260 Panthalassa and Palaeotethys sea would translate into  $\sim 6\text{-}8$  psu salinity variation.  
261 Assuming that the Palaeotethys had normal marine salinities like the modern ocean  
262 ( $\sim 35$  psu salinity), the Panthalassa sea would have salinities of  $27\text{-}29$  psu salinity.

263 Continental runoff lowering seawater  $\delta^{18}\text{O}$  may also explain why comparably low  
264  $\delta^{18}\text{O}_{\text{apatite}}$  values are measured in South China and Australia in the Pragian. The Pragian  
265 was a time when marine sediment initially occurred after the Guangxi Orogeny, and all  
266 Pragian data from South China are from the Dashatian section, which is dominated by  
267 terrigenous siliciclastics interbedded with few carbonate beds, representing a near  
268 coastal setting (Wang et al., 2016; Qiao et al., 2021). Thus, this section likely was  
269 influenced by enhanced freshwater input, resulting in lower seawater  $\delta^{18}\text{O}$  and  $\delta^{18}\text{O}_{\text{apatite}}$   
270 values. Accordingly, the data from this section were not considered for  
271 palaeotemperature reconstruction. All Late Devonian and Early Carboniferous  
272  $\delta^{18}\text{O}_{\text{apatite}}$  data are from the Palaeotethys ocean. Thus, it is not surprising that regional  
273 differences in  $\delta^{18}\text{O}_{\text{apatite}}$  are less obvious (Fig. 3A, B; Fig. 4).

274 The above observations indicate that Devonian oceans may have been  
275 characterized by significant differences in  $\delta^{18}\text{O}_{\text{seawater}}$ , with epicontinental seas having  
276 distinctly lower  $\delta^{18}\text{O}_{\text{seawater}}$  than the open ocean as consequence of the input of  
277 freshwater. An average  $\delta^{18}\text{O}_{\text{seawater}}$  value of  $-1\text{‰}$  is usually assumed for time intervals  
278 without major ice caps in high latitudes. However, this assumption is an  
279 oversimplification (Judd et al. 2020) as documented in the variability of seawater  $\delta^{18}\text{O}$   
280 in the modern oceans (Schmidt et al., 1999). Thus, reconstruction of deep time ocean  
281 temperatures and/or ice volume should preferentially be based on oxygen isotope data  
282 from open ocean settings.

283 Despite regional differences in  $\delta^{18}\text{O}_{\text{apatite}}$  between palaeocontinents (Fig. 3A, B) or  
284 even between sections from one paleocontinent (e.g. Girard et al., 2020) (Fig. 3A, B),  
285 the Devonian  $\delta^{18}\text{O}_{\text{apatite}}$  records from South China and Europe generally show similar  
286 secular trends characterized by a pronounced increase in  $\delta^{18}\text{O}_{\text{apatite}}$  during the Pragian  
287 to early Emsian to Eifelian followed by significant decrease during the late  
288 Eifelian/Givetian to Frasnian, and a further rise starting in the early Famennian,  
289 accelerating in the earliest Carboniferous (Fig. 3A, B). Interestingly, similar long-term  
290 oxygen isotope trends are also seen in the  $\delta^{18}\text{O}$  record of well-preserved brachiopod  
291 calcite measured from multiple low latitude continents (Fig. 3C, van Geldern et al.,  
292 2006). These parallel trends measured on brachiopod calcite and conodont apatite  
293 deriving from various low latitude locations (Fig. 3) can serve as evidence supporting  
294 the inference that the primary oxygen isotope signals are well preserved in most of the  
295 South China samples and the observed changes in  $\delta^{18}\text{O}$  mainly record global climatic  
296 changes. Since the regional differences in seawater  $\delta^{18}\text{O}$  complicate absolute  
297 temperature estimation, we only compare the temperature records from two low  
298 latitudinal regions (  $0\text{-}15^\circ\text{S}$ ) within Palaeotethys (South China and Europe).

299 Applying the temperature equation of Lécuyer et al. (2013) and assuming a  $\delta^{18}\text{O}$   
300 value for Devonian seawater of  $-1\text{‰}$  VSMOW, the  $\delta^{18}\text{O}_{\text{apatite}}$  records suggest cooling  
301 of tropical seawater by  $\sim 8$  to  $10^\circ\text{C}$  (Fig. 4) during the Pragian to Emsian/Eifelian  
302 followed by  $8$  to  $10^\circ\text{C}$  (Fig. 4) warming during the Eifelian/Givetian to Frasnian. The

303 European record shows a moderate ~5 °C temperature decrease during the Famennian.  
304 Unfortunately, coeval data from South China are sparse, hindering a direct comparison  
305 between the two regions. However, both records suggest further cooling during the  
306 earliest Carboniferous (Chen et al., 2021; Fig. 4). The parallel palaeotemperature trends  
307 suggest that the Devonian climate variations occurred globally.

308

## 309 **5.2 Potential drivers of Devonian climate change**

310 It is generally assumed that variations in atmospheric CO<sub>2</sub> concentration played a  
311 key role in controlling changes in Earth's climate over the Phanerozoic Eon (Royer et  
312 al., 2004; Came et al., 2017; Mills et al., 2019). Primary carbon sources to the  
313 atmosphere are CO<sub>2</sub> emitted by tectonic and volcanic processes and oxidative  
314 weathering of organic carbon, while CO<sub>2</sub> sinks are silicate weathering and burial of  
315 organic carbon. CO<sub>2</sub> emission is linked to the intensity of tectonic or volcanic activities  
316 which are generally represented over long timescales by the rate of material generation  
317 and subduction, based on ridge production rate and lengths of arcs (Van Der Meer et al.,  
318 2014; Mills et al., 2017; Cao et al., 2017). Silicate weathering depends on multiple  
319 factors including runoff, temperature, and physical erosion rates (Royer, 2014;  
320 Godd ris et al., 2014), which in turn would be influenced by changes in topography,  
321 paleogeography, climate, and terrestrial plant coverage.

322 Enhanced silicate weathering due to the advent of terrestrial vascular plants (Algeo  
323 et al., 1995, 2001; Algeo and Scheckler, 1998; Lenton et al., 2018) has been considered  
324 as major trigger of the *p*CO<sub>2</sub> decrease during the Devonian, which resulted in the  
325 transition from the Early Paleozoic “greenhouse” to Late Paleozoic “icehouse”(Qie et  
326 al., 2019). However, the exact timing of events is uncertain. Proxy *p*CO<sub>2</sub> data and  
327 modelling studies have suggested that cooling started in the Emsian at ca. 400 Ma or  
328 even earlier (Royer et al., 2014; Foster et al., 2017; Lenton et al., 2018), while other  
329 authors suggested a later onset in the Middle (Givetian) to Late Devonian following the  
330 advent of forests and deeper root systems (Stein et al., 2012; Giesen and Berry, 2013).  
331 The oxygen isotope based palaeotemperature reconstructions indicate that the first  
332 Devonian climatic cooling took place in Pragian to Emsian times, followed by climatic

333 warming during the Givetian and Frasnian interval, and further cooling occurring again  
334 in the Famennian (Fig. 4). In the following sections, the Devonian climate evolution  
335 and the potential driving mechanism(s) will be discussed.

336

### 337 **5.2.1 Was Early Devonian cooling triggered by the radiation of early rooted plants?**

338 The South China and European palaeotemperature records (Fig. 4) suggest that  
339 cooling occurred in the Early Devonian, with a more stable climate dominating the late  
340 Emsian to Eifelian which is generally in agreement with modeling based  $p\text{CO}_2$   
341 predictions (Fig. 5). Long-term climatic cooling is usually interpreted as resulting either  
342 from increased  $\text{CO}_2$  consumption via silicate weathering or reduced  $\text{CO}_2$  degassing  
343 from tectonic and volcanic activities. In particular, low-latitude arc-continent collisions  
344 or emplacement of larger igneous provinces would significantly promote exhumation  
345 and erosion of mafic and ultramafic rocks (Cox et al., 2016; Macdonald et al., 2019),  
346 which are effective at consuming  $\text{CO}_2$  via chemical weathering (McKenzie et al., 2016;  
347 Hartmann et al., 2014; Schopka et al., 2011). Fresh exposure of ophiolites following  
348 arc-continent collisions or of basalt after LIP emplacement may significantly accelerate  
349 silicate weathering and carbon sequestration (Cox et al., 2016; Macdonald et al., 2019),  
350 especially if occurring in tropical latitudes. However, the low active suture length and  
351 LIP area reconstructed for the Pragian-Emsian (Macdonald et al., 2019; Fig. 5) suggest  
352 that silicate weathering from both was likely ineffective in removing  $\text{CO}_2$  from the  
353 atmosphere. In addition, although reconstructions suggest an overall decrease in the  
354  $\text{CO}_2$  outgassing rate from mid ocean ridges or continental arc activity from the  
355 Ordovician to Carboniferous (Mckenzie et al., 2016; Cao et al., 2017; Mills et al., 2017,  
356 2019), short-term outgassing rates are extremely difficult to calculate, so a reduced  
357 tectonic degassing flux cannot be clearly implicated in Pragian-Emsian cooling.

358 We suggest that Early Devonian cooling may be a consequence of accelerating  
359 silicate weathering initiated by the occurrence of the early rooted vascular plants.  
360 According to Algeo et al. (1995, 2001), early vascular plants prior to the Middle  
361 Devonian were mainly herbaceous, relatively small in stature (<1 m) and ecologically  
362 restricted to specific habitats. Roots or rhizomes of these early plants are rarely found

363 and/or incompletely preserved (Morris et al., 2015). However, the impact of these early  
364 plants on soil production and continental silicate weathering could be substantial (Algeo,  
365 et al., 2001; Xue et al., 2016). For example, recent paleobotanical studies document a  
366 complex rhizome system for the lycopsid *Drepanophycus* (Xue et al., 2016) and rooting  
367 systems for lycophytes (Matsunaga and Tomescu, 2016) almost simultaneously  
368 occurring in South China and North America in the Pragian (Fig. 5). Similar rhizomes  
369 or rooting structures were also observed in Lochkovian to Emsian sediments of  
370 Southern Britain (Hillier et al., 2008) and Bathurst Island/Arctic Canada (Gensel et al.,  
371 2001). Larger and deeper root systems capable of penetrating downward into the  
372 substrate by ~1 m are reported from Emsian strata in Canada, although the parent plant  
373 is unclear (Elick et al., 1998).

374 These findings suggest that rhizomes or rooting systems having the capability of  
375 producing rooted paleosols (Xue et al., 2016) may have been well established since the  
376 Pragian. This further suggests that relatively complex plant–soil interactions already  
377 existed prior to the advent of forests and deep root systems (Algeo, et al., 2001; Xue et  
378 al., 2016; Matsunaga and Tomescu, 2016). Additionally, advanced root systems in the  
379 Pragian were coincident with a significant increase in spore and mega plant fossil  
380 diversities (Fig. 5, Wang et al., 2000, Cascales-Minana, 2016, Xue et al., 2018, Shen et  
381 al., 2020), as well as a significant expansion of global vegetation cover, estimated to be  
382 from 10 to 30% of modern coverage (Fig. 5; Simon et al., 2007). Furthermore, a  
383 pronounced increase in plant biomass and terrestrial organic carbon burial is evidenced  
384 by the development of coal-like accumulations in multiple localities (Wehrmann et al.,  
385 2005, Kennedy et al., 2013, Morris et al., 2011; Nelsen et al., 2016) and high  $\delta^{13}\text{C}_{\text{carb}}$   
386 values in coeval marine carbonates (Fig. 6, Buggisch and Joachimski, 2006).

387 An increased influence of Early Devonian vegetation and its root systems on  
388 continental weathering can also be inferred from multiple lines of indirect evidence, for  
389 example significant changes in river systems characterized by a shift from braided to  
390 meandering streams (Davies and Gibling, 2010; Gibling and Davies, 2012), and a  
391 prominent increase in mud deposition in alluvial plain system allowing more complete  
392 weathering of primary minerals (McMahon and Davies, 2018) under a context of higher

393 weathering intensity in response to the expansion of land plants (Lipp et al., 2021). Mo  
394 isotope and I/Ca data from South China and North American sections, as well as isotope  
395 mass balance models for global sedimentary  $\delta^{13}\text{C}$ , indicate that a major oxygenation  
396 pulse took place in the Early-Middle Devonian (ca. 400 Ma) (Dahl et al., 2010; Krause  
397 et al., 2018; He et al., 2019, Lu et al., 2018) with excess  $\text{O}_2$  likely produced by enhanced  
398 burial of terrestrial biomass due to the higher C/P ratio of early land plants, coupled  
399 with a plant-driven P weathering increase promoted the burial of marine organic carbon  
400 (Lenton et al., 2016).

401 These ideas suggest that terrestrial as well as marine productivity and biomass may  
402 have substantially increased since the Pragian. In conjunction with the advent of root  
403 systems and the co-evolution of symbiotic mycorrhizal fungi (Remy et al., 1994;  
404 Strullu-Derrien et al., 2014; Mills et al., 2018), the Early Devonian vegetation may have  
405 considerably enhanced silicate weathering and organic carbon burial, promoting  
406 sequestration of atmospheric  $\text{CO}_2$ , culminating in climatic cooling. The COPSE model  
407 as shown in Figure 5 (Tostevin and Mills, 2020) incorporates the essentials of the plant  
408 root hypothesis but assumes that the significant radiation of rooted terrestrial vegetation  
409 occurred between ~400 and ~380 Ma (Lenton et al., 2018). The model predictions  
410 therefore indicate that Early Devonian cooling started at 400 Ma. Alternatively,  
411 assuming an earlier onset of the radiation of rooted vegetation at ~410 Ma, the COPSE  
412 model predicts a more comparable  $p\text{CO}_2$  and oxygen isotopic based temperature record  
413 (Fig. 5).

414

### 415 **5.2.2 Givetian–Frasnian warming triggered by metamorphic $\text{CO}_2$ degassing?**

416 Climate warming during the late Givetian to Frasnian is unexpected, since the  
417 Middle Devonian is generally considered as a time interval with the earliest forests with  
418 deep root systems and a complex floral community (Stein et al., 2007; 2012). However,  
419 a significant climatic warming episode has been identified from both conodont apatite  
420 and brachiopod calcite  $\delta^{18}\text{O}$  records (Fig. 5; Joachimski et al., 2009; van Geldern et al.  
421 2006). In addition, the broader latitudinal distribution of tropical floras and miospores,  
422 indicating a weak latitudinal temperature gradient is considered as a biosphere response

423 to this warming (Streele et al., 2000). Van Geldern et al. (2006) suggested that intensified  
424 CO<sub>2</sub> outgassing from midocean ridges as inferred from the high sea-level (Johnson et  
425 al., 1985) and/or island arc volcanism, was a potential reason for this warming event.  
426 However, long-term reconstructions of CO<sub>2</sub> outgassing from mid-ocean ridges or  
427 continental arc activity tend to show a decreasing or flat trend during the Middle-Late  
428 Devonian transition (Mckenzie et al., 2016; Cao et al., 2017; Mills et al., 2017). The  
429 abrupt rise in tropical active suture length and LIP area (Macdonald et al., 2019; Fig. 5)  
430 further suggest that a reduction in mafic and ultramafic rock weathering was unlikely  
431 to be the cause of this warming.

432 Stewart and Ague (2018) proposed that metamorphic CO<sub>2</sub> degassing derived from  
433 fluid infiltration-driven decarbonation during the Acadian Orogeny (Fig. 5 ca. 390-375  
434 Ma) may have injected a total flux of  $0.7\sim 2.5 \times 10^{19}$  mol CO<sub>2</sub> to the atmosphere, resulting  
435 in significant global warming and the “Taghanic bio-crisis”. The proposed CO<sub>2</sub>  
436 injection is thought to have started at 390 Ma coinciding with climate warming as  
437 suggested by the  $\delta^{18}\text{O}_{\text{apatite}}$  records. Interestingly, this climate warming coincides with  
438 a significant sea level rise observed in both South China and North America (Fig. 6,  
439 Johnson et al., 1985; Ma et al., 2017). The rising sea level could be interpreted to  
440 indicate the melting of ice masses (Elrick et al., 2009), however no direct glacial  
441 deposits have been observed at this time. To assess the likelihood of Acadian degassing  
442 driving this warming, we incorporated enhanced CO<sub>2</sub> degassing into the COPSE model  
443 run. We increased the model degassing rate by 33% over a 10 Myr period corresponding  
444 to the Acadian orogenesis, which gives an additional CO<sub>2</sub> input at the upper end of the  
445 estimates of Stuart and Ague (2018).  $p\text{CO}_2$  proxy data are highly scattered but do  
446 broadly confirm a minor increase over the degassing interval, as predicted by the  
447 COPSE model. However, the model does not reproduce the degree of warming that is  
448 indicated by the  $\delta^{18}\text{O}$  records.

449

### 450 **5.2.3 Famennian cooling: the advent of seed plants or Arc-continent collisions?**

451 The  $\delta^{18}\text{O}_{\text{apatite}}$  record indicates two abrupt and transient cooling events across the  
452 Frasnian-Famennian boundary, which have been reported in multiple low latitude-



453 sections (Joachimski and Buggisch, 2002; Balter et al., 2008; for summary see Huang  
454 et al. 2018) and are attributed to a transient increase of organic carbon burial  
455 (Joachimski and Buggisch, 2002). However, these short-term changes are not well  
456 defined in the long-term records (Fig. 4). The long-term  $\delta^{18}\text{O}_{\text{apatite}}$  record indicates  
457 cooling starting in the early Famennian and accelerating into the earliest Carboniferous  
458 (Fig. 4).

459 The Famennian cooling coincided with the origin and diversification of seed plants  
460 (Fig. 5; Algeo et al., 1995), alongside the occurrence of more complex vascular systems  
461 (Meyer-Berthaud et al., 1999; Hilton et al., 2003; Rowe and Speck, 2005; Wang and  
462 Liu, 2015), diversification in leaf morphologies (Boyce and Knoll, 2002; Xue et al.,  
463 2015) as well as a significant increase in plant height (Mosbrugger, 1990; Dilcher et al.,  
464 2004; Meyer-Berthaud et al., 2010). The advent and diversification of seed plants  
465 (Prestianni and Gerrienne, 2010) was of particular importance, since the reproduction  
466 of seed plants is fully independent of water, enabling them to colonize drier uplands  
467 (Algeo and Scheckler, 1998; Fairon-Demaret and Hartkopf-Fröder, 2004, Taylor et al.,  
468 2009). Consequently, vegetation coverage dramatically increased during the Famennian  
469 (Simon et al., 2007, Algeo and Scheckler, 2010). The taller, leafier plants had to develop  
470 more advanced rooting systems and hosted more symbionts in order to obtain more  
471 water and nutrients (Raven and Edwards, 2001). As a result, the root systems of  
472 Famennian plants became larger (10 to 15 cm in diameter, up to 1.5 m in deep), more  
473 complicated in morphology (Driese and Mora, 2001), with the total root mass, a  
474 parameter regarded as a reliable proxy for pedogenic weathering intensity, dramatically  
475 raising to near ~50% of modern levels (Algeo and Scheckler, 2010). These significant  
476 innovations in vegetation may have resulted again in a significant promotion of  
477 terrestrial weathering.

478 It is interesting to note that reconstructions of active suture length in the tropics  
479 indicate an abrupt increase to ~3,000 kilometers in the latest Frasnian and Famennian  
480 (Macdonald et al., 2019). Basalt weathering following the emplacement of LIPs in the  
481 tropics has a similar climatic effect as low-latitude arc-continent collisions (Macdonald  
482 et al., 2019; Park et al., 2021). The emplacement of the Viluy and Kola-Dnieper LIPs

483 are dated as Middle to Late Devonian (Kusznir et al., 1996; Wilson and Lyashkevich,  
484 1996, Courtillot et al., 2010, Kravchinsky et al., 2012), with the estimated LIP exposed  
485 area increasing substantially over 385-380 Ma (Fig. 5), ranking this period as a peak  
486 interval of basalt exposure (Macdonald et al., 2019). Weathering of freshly exposed  
487 basalts or ophiolites may have provided a mechanism to drive climatic cooling (Dessert  
488 et al., 2003). However, the increase in active suture length and basalt areas started in  
489 the Givetian (380 Ma) and late Frasnian (375 Ma), respectively, during warming  
490 climatic conditions and 12 and 7 Ma before the onset of Famennian cooling (Fig. 5).  
491 This suggests that weathering of basalts or ophiolites did not immediately result in  
492 climatic cooling. However, the relatively large basalt and ophiolite exposure areas  
493 alongside with declining tectonic CO<sub>2</sub> degassing imply that these factors may still  
494 possibly make a considerable contribution to the Famennian cooling, which culminated  
495 in a short glaciation in the late Famennian (Caputo, 1985; Caputo et al., 2008).

496 In summary, enhanced silicate weathering in association with the advent of seed  
497 plants and their deeper and complicated root systems could have played a leading role  
498 in driving the Famennian cooling, which was further reinforced by weathering of  
499 ophiolites and basalts. The combined effect of these events would have significantly  
500 accelerated removal of CO<sub>2</sub> from the atmosphere (Berner et al., 2003), ultimately  
501 leading to the global climate transition from the Early Paleozoic Greenhouse to the Late  
502 Paleozoic Icehouse. The continued expansion of land plants and the weathering of  
503 volcanic terranes were already included in the COPSE model run (in a basic form), and  
504 it is capable of generating a CO<sub>2</sub> record that is consistent with the proxy data and  
505 predicts cooling over the Famennian. However, as above, the model does not recreate  
506 the large changes in tropical temperatures that are reconstructed from the δ<sup>18</sup>O record.  
507 Given that the COPSE model is a simple nondimensional box model, the tropical  
508 temperature change is calculated from the global average temperature assuming a  
509 constant poleward heat transport by multiplying the global temperature change by a  
510 constant factor of  $\frac{2}{3}$  (see Mills et al., 2019). This is an oversimplification as the polar  
511 amplification factor itself appears to be dynamic (Valdez et al., 2021), which could

512 change the assumed model ‘tropical’ temperatures by several degrees.

513

## 514 **6. Conclusions**

515 Multiple Devonian oxygen isotope records from different low latitude areas  
516 illustrate a Devonian climate characterized by cooling during the Pragian to Emsian,  
517 significant warming during the Givetian to Frasnian, and cooling starting in the  
518 Famennian and accelerating in the earliest Carboniferous. A close comparison of the  
519 climatic variations and vegetation innovation events suggests that the Pragian to  
520 Emsian and Famennian cooling corresponded to the first establishment of vascular plant  
521 root-soil interactions, and later to the advent of seed plants in conjunction with the  
522 development of deep and morphological complex root systems. These dynamic  
523 Devonian climatic changes add complexity to a more generally assumed gradual  
524 decrease in atmospheric CO<sub>2</sub> resulting from the rise of the Devonian vegetation. In  
525 addition, tectonic and volcanic activities are suggested to have played an important role  
526 in driving the Devonian climate, with weathering of freshly exposed ophiolites and  
527 basalts consuming CO<sub>2</sub> and thus driving climatic cooling in the Late Devonian, whereas  
528 contact metamorphism produced by orogenic activities likely contributed to a CO<sub>2</sub> rise  
529 and climatic warming in the Middle Devonian.

530

## 531 **Acknowledgements**

532 This study was financially supported by the Strategic Priority Research Program of  
533 Chinese Academy of Sciences (Grant Nos. XDB26000000, XDB18000000) and the  
534 Natural Science Foundation of China (Grant Nos. 41872003, 41302019, 91955201,  
535 41772004), M. X. acknowledges students Zhang Yubo, Zong Pu, Lü Dan, and Zhang  
536 Meiqiong for their help in the fieldwork, Zhang Meiqiong is especially thanked for her  
537 help for processing conodont specimens in the lab. BJWM acknowledges the UK  
538 Natural Environment Research Council for funding (NE/S009663/1), We thank three  
539 reviewers for their constructive comments that significantly improved the quality of  
540 this manuscript.

541

542 **References**

- 543 Algeo, T. J., Heckel, P.H., 2008. The Late Pennsylvanian Midcontinent Sea of North America: a review. .  
544 Palaeogeography, Palaeoclimatology, Palaeoecology 268, 205–221.
- 545 Algeo, T. J., Scheckler, S. E., 1998. Terrestrial-marine teleconnections in the Devonian: links between the evolution  
546 of land plants, weathering processes, and marine anoxic events. Philosophical Transactions of the Royal  
547 Society B: Biological Sciences 353(1365), 113–130.
- 548 Algeo, T. J., Scheckler, S., 2010. Land Plant Evolution and Weathering Rate Changes in the Devonian. Journal of  
549 Earth Science 21, 75–78.
- 550 Algeo, T. J., Berner, R., Maynard, J. and Scheckler, S., 1995. Late Devonian oceanic anoxic events and biotic crises:  
551 "Rooted" in the evolution of vascular plants. GSA Today 5(45), 64–66.
- 552 Algeo T. J., Scheckler, S. E., Maynard, J. B., 2001. Effects of the Middle to Late Devonian spread of vascular land  
553 plants on weathering regimes, marine biotas, and global climate P.G. Gensel, D. Edwards (Eds.), Plants  
554 Invade the Land: Evolutionary and Environmental Perspectives, Columbia University Press, New  
555 York (2001), pp. 213–236
- 556 Algeo, T. J., Chen, Z. Q., Fraiser, M. L. and Twitchett, R. J., 2011. Terrestrial–marine teleconnections in the collapse  
557 and rebuilding of Early Triassic marine ecosystems. Palaeogeography, Palaeoclimatology, Palaeoecology  
558 308(1–2), 1–11.
- 559 Balter, V., Renaud, S., Girard, C., Joachimski, M. M., 2008. Record of climate-driven morphological changes in 376  
560 Ma Devonian fossils. Geology 36, 907–910.
- 561 Berner, R. A., 1997. The Rise of Plants and Their Effect on Weathering and Atmospheric CO<sub>2</sub>. Science, 276(5312):  
562 544–546.
- 563 Berner, R. A., 2003. The rise of trees and their effects on Paleozoic atmospheric CO<sub>2</sub> and O<sub>2</sub>. Comptes Rendus  
564 Geosciences 335(16), 1173–1177.
- 565 Boyce, C. K., Knoll, A. H., 2002. Evolution of developmental potential and the multiple independent origins of  
566 leaves in Paleozoic vascular plants. Paleobiology 28, 70–100.
- 567 Buggisch, W. and Joachimski, M. M., 2006. Carbon isotope stratigraphy of the Devonian of Central and Southern  
568 Europe. Palaeogeography, Palaeoclimatology, Palaeoecology 240(1–2), 68–88.
- 569 Buggisch, W., Joachimski, M. M., Sevastopulo, G. and Morrow, J. R., 2008. Mississippian  $\delta^{13}\text{C}_{\text{carb}}$  and conodont  
570 apatite  $\delta^{18}\text{O}$  records -- Their relation to the Late Palaeozoic Glaciation. Palaeogeography,  
571 Palaeoclimatology, Palaeoecology, 268(3–4): 273–292.
- 572 Came, R. E., Eiler, J. M., Veizer, J., Azmy, K., Brand, U. and Weidman, C. R., 2007. Coupling of surface temperatures  
573 and atmospheric CO<sub>2</sub> concentrations during the Palaeozoic era. Nature 449(7159), 198–201.
- 574 Cao, W., Lee, C. T. A., Lackey, J. S., 2017. Episodic nature of continental arc activity since 750 Ma: A global  
575 compilation. Earth and Planetary Science Letters 461, 85–95.
- 576 Caputo, M. V., 1985. Late Devonian glaciation in South America. Palaeogeography, Palaeoclimatology,  
577 Palaeoecology 51(1), 291–317.
- 578 Caputo, M. V., de Melo, J. H. G., Streef, M., Isbell, J. L., 2008. Late Devonian and Early Carboniferous glacial  
579 records of South America. Geological Society of America Special Papers 441, 161–173.
- 580 Cascales-Miñana, B., 2016. Apparent changes in the Ordovician–Mississippian plant diversity. Review of  
581 Palaeobotany and Palynology 227 (Supplement C), 19–27.
- 582 Chen, B., Joachimski, M.M., Shen, S.-Z., Lambert, L.L., Lai, X.-L., Wang, X.-D., Chen, J. and Yuan, D.-X., 2013.  
583 Permian ice volume and palaeoclimate history: Oxygen isotope proxies revisited. Gondwana Research,

584 24(1): 77-89.

585 Chen, B., Joachimski, M.M., Wang, X.D., Shen, S. Z., Qi, Y. P. and Qie, W.k., 2016. Ice volume and paleoclimate  
586 history of the Late Paleozoic Ice Age from conodont apatite oxygen isotopes from Naqing (Guizhou,  
587 China). *Palaeogeography, Palaeoclimatology, Palaeoecology*, 448: 151–161.

588 Chen, B., Chen, J. T., Qie, W. K., Huang P., He,T., Joachimski, M.M., Regelous, M., Pogge von Strandmann, P.  
589 A.E., Liu, J., Wang X. D., Montañez, I. P., Algeo, T. J., 2021. Was climatic cooling during the earliest  
590 Carboniferous driven by expansion of seed plants? *Earth and Planetary Science Letters* 565: 116953

591 Chen, D., Tucker, M. E., Zhu, J., Jiang, M., 2001a. Carbonate sedimentation in a starved pull-apart basin, Middle to  
592 Late Devonian, southern Guilin, South China. *Basin Research* 13(2), 141–167.

593 Chen, D., Tucker, M. E., Jiang, M., Zhu, J., 2001b. Long-distance correlation between tectonic-controlled, isolated  
594 carbonate platforms by cyclostratigraphy and sequence stratigraphy in the Devonian of South China.  
595 *Sedimentology* 48, 57–78.

596 Chen, D., Tucker, M. E, Zhu, J. Q, Jiang, M., 2002. Carbonate platform evolution: From a bioconstructed platform  
597 margin to and-shoal system (Devonian), Guilin, South China. *Sedimentology* 49, 737–764.

598 Chen, J., Shen, S. Z., Li, X. H., Xu, Y. G., Joachimski, M. M., Bowring, S. A., Erwin, D. H., Yuan, D.X., Chen, B.,  
599 Zhang, H., Wang, Y., Cao, C. Q., Zheng, Q. F., Mu, L., 2016. High-resolution SIMS oxygen isotope  
600 analysis on conodont apatite from South China and implications for the end-Permian mass extinction  
601 *Palaeogeography, Palaeoclimatology, Palaeoecology* 448, 26-38.

602 Chen, X., Fan, J. X., Chen, Q., Tang, L. Hou, X. D., 2014. Toward a stepwise Kwangsi Orogeny. *Science China:  
603 Earth Sciences* 57(3), 379–387.

604 Cox, G. M., Halverson, G. P., Stevenson, R. K., Vokaty, M., Poirier, A., Kunzmann, M., Li, Z. X., Denysyn, S. W.,  
605 Strauss, J. V., Macdonald, F. A., 2016. Continental flood basalt weathering as a trigger for Neoproterozoic  
606 Snowball Earth. *Earth and Planetary Science Letters* 446, 89–99.

607 Cox, G. M., Lyons, T. W., Mitchell, R. N., Hasterok, D., Gard, M., 2018. Linking the rise of atmospheric oxygen to  
608 growth in the continental phosphorus inventory. *Earth and Planetary Science Letters* 489, 28–36.

609 Courtillot, V., Kravchinsky, V. A., Quidelleur, X., Renne, P. R., Gladkochub, D. P., 2010. Preliminary dating of the  
610 Viluy traps (Eastern Siberia): eruption at the time of Late Devonian extinction events? *Earth and Planetary  
611 Science Letters* 300, 239–245.

612 Dahl, T. W., Hammarlund, E. U., Anbar, A. D., Bond, D. P. G., Gill, B. C., Gordon, G. W., Knoll, A. H., Nielsen,  
613 A.T., Schovsbo, N. H., Canfield, D. E., 2010. Devonian rise in atmospheric oxygen correlated to the  
614 radiations of terrestrial plants and large predatory fish. *Proceedings of the National Academy of Sciences*  
615 107(42), 17911–17915.

616 Davies, N. S. and Gibling, M. R., 2010. Cambrian to Devonian evolution of alluvial systems: The sedimentological  
617 impact of the earliest land plants. *Earth Science Reviews* 98(3), 171–200.

618 Dessert, C., Dupré, B., Gaillardet, J., François, L. M., Allègre, C. J., 2003. Basalt weathering laws and the impact of  
619 basalt weathering on the global carbon cycle. *Chemical Geology* 202 (3-4), 257–273.

620 Dilcher, D. L., Lott, T. A., Wang, X., Wang, Q., 2004. A history of tree canopies. In: Lowman, M. D., Rinker, H.  
621 B. (Eds.), *Forest Canopies*. Elsevier, pp. 118–137.

622 DiMichele, W. A. and Bateman, R. M., 1996. Plant paleoecology and evolutionary inference: two examples from the  
623 Paleozoic. *Review of Palaeobotany and Palynology* 90(3), 223–247.

624 Driese, S.G., Mora, C.I. 2001. Diversification of Siluro-Devonian plant traces in paleosols and influence on estimates  
625 of paleoatmospheric CO<sub>2</sub> levels *Plants Invade the Land: Evolutionary and Environmental Perspectives*,  
626 Columbia University Press, New York (2001), pp. 237–253

627 Edwards, D., Cherns, L., Raven, J. A., 2015. Could land-based early photosynthesizing ecosystems have

628 bioengineered the planet in mid-Palaeozoic times? *Palaeontology* 58(5), 803–837.

629 Elrick, M., Berkyová, S., Klapper, G., Sharp, Z., Joachimski, M., Frýda, J., 2009. Stratigraphic and oxygen isotope  
630 evidence for My-scale glaciation driving eustasy in the Early–Middle Devonian greenhouse world.  
631 *Palaeogeography, Palaeoclimatology, Palaeoecology* 276(1–4), 170–181.

632 Elick, J. M., Driese, S. G., Mora, C. I., 1998. Very large plant and root traces from the Early to Middle Devonian:  
633 Implications for early terrestrial ecosystems and atmospheric  $p(\text{CO}_2)$ . *Geology* 26 (2), 143–146.

634 Ernst, R. E., Rodygin, S. A., Grinev, O. M., 2020. Age correlation of Large Igneous Provinces with Devonian biotic  
635 crises. *Global and Planetary Change* 185, 103097

636 Foster, G. L., Royer, D. L., Lunt, D. J., 2017. Future climate forcing potentially without precedent in the last 420  
637 million years. *Nature Communications* 8, 14845.

638 Fäyren-Demaret, M., Hartkopf-Fröer, C., 2004. Late Famennian plant mesofossils from the Refrath 1 Borehole  
639 (Bergisch Gladbach-Paffrath Syncline; Ardennes-Rhenish Massif, Germany). *Courier Forschungsinstitut*  
640 *Senckenberg Senckenberg* 251, 89–121.

641 Garbelli, C., Angiolini, L., and Shen, S. Z., 2017, Biomineralization and global change: A new perspective for  
642 understanding the end-Permian extinction: *Geology* 45, 19–22.

643 Gerrienne, P., Gensel, P. G., Strullu-Derrien, C., Lardeux, H., Steemans, P., Prestianni, C., 2011. A simple type of  
644 wood in two Early Devonian plants. *Science* 333, 837.

645 Gibling, M. R. and Davies, N. S., 2012. Palaeozoic landscapes shaped by plant evolution. *Nature Geoscience*, 5: 99.

646 Gensel, P. G., Kotyk, M. E., Basinger, J. F., 2001. Morphology of above- and below-ground structures in Early  
647 Devonian (Pragian–Emsian) plants. Gensel, P. G., Edwards, D. (Eds.), *Plants Invade the Land:*  
648 *Evolutionary and Environmental Perspectives*, Columbia University Press, New York (2001), pp. 83–102

649 Giesen, P. and Berry, C. M., 2013. Reconstruction and Growth of the Early Tree Calamophyton (Pseudosporochnales,  
650 Cladoxylopsida) Based on Exceptionally Complete Specimens from Lindlar, Germany (Mid-Devonian):  
651 Organic Connection of Calamophyton Branches and Duisbergia Trunks. *International Journal of Plant*  
652 *Sciences*, 174(4): 665–686.

653 Girard, C., Cornée, J., Joachimski, M. M., Charruault, A., Dufour, A., Renaud, S., 2020. Paleogeographic differences  
654 in temperature, water depth and conodont biofacies during the Late Devonian. *Palaeogeography,*  
655 *Palaeoclimatology, Palaeoecology*, 549:108852

656 Gradstein, F. M., Ogg, J. G., Schmitz, M., Ogg, G. A. (Eds.), *Geologic Time Scale 2012*. Cambridge University Press,  
657 London, pp. 1–206.

658 Goddérís, Y., Donnadiou, Y., Le Hir, G., Lefebvre, V., Nardin, E., 2014. The role of palaeogeography in the  
659 Phanerozoic history of atmospheric  $\text{CO}_2$  and climate. *Earth Science Reviews*, 128: 122–138.

660 Goddérís, Y., Donnadiou, Y., Tombozafy, M., Dessert, C., 2008. Shield effect on continental weathering: Implication  
661 for climatic evolution of the Earth at the geological timescale. *Geoderma*, 145(3): 439–448.

662 Hartmann, J., Moosdorf, N., Lauerwald, R., Hinderer, M., West, A. J., 2014. Global chemical weathering and  
663 associated P-release — The role of lithology, temperature and soil properties. *Chemical Geology*, 363:  
664 145–163.

665 He, R., Lu, W., Junium, C. K., Ver Straeten, C. A., Lu, Z., 2019. Paleo-redox context of the Mid-Devonian  
666 Appalachian Basin and its relevance to biocrises. *Geochimica et Cosmochimica Acta*, 287: 328–340.

667 Heckel, P.H., 1977. Origin of phosphatic black shale facies in Pennsylvanian cyclothem of Mid-Continent North  
668 America. *American Association of Petroleum Geologists Bulletin* 61, 1045–1068.

669 Hillier, R. D., Edwards, D, Morrissey, L, B., 2008. Sedimentological evidence for rooting structures in the Early  
670 Devonian Anglo-Welsh Basin (UK), with speculation on their producers. *Palaeogeography,*  
671 *Palaeoclimatology, Palaeoecology* 270(3). 366–380

672 Hilton, J., Geng, B., Kenrick, P., 2003. A Novel Late Devonian (Frasnian) Woody Cladoxylopsid from China.  
673 International Journal of Plant Sciences –International Journal of Plant Sciences, 164: 793–805.

674 Huang, C., Joachimski, M. M., Gong, Y., 2018. Did climate changes trigger the Late Devonian Kellwasser Crisis?  
675 Evidence from a high-resolution conodont  $\delta^{18}\text{O}_{\text{PO}_4}$  record from South China. Earth and Planetary Science  
676 Letters, 495: 174–184.

677 Huang, C., Gong, Y.M., 2016. Timing and patterns of the Frasnian–Famennian event: evidences from high-resolution  
678 conodont biostratigraphy and event stratigraphy at the Yangdi section, Guangxi, South China.  
679 Palaeogeography, Palaeoclimatology, Palaeoecology 448: 317–338.

680 Ihaka, R., Gentleman, R., 1996. R: a language for data analysis and graphics. Journal of Computational and Graphical  
681 Statistics. 5, 299–314.

682 Jin, S. Y., Shen, A. J., Chen, Z. L., Lu, J. M., Wei, M., Wang, Y. Q., Xie, F., 2005. Mixed Biostratigraphy of Devonian  
683 in Wenshan, Yunnan Petroleum Industry Press Beijing pp 1–181.

684 Joachimski, M.M. and Buggisch, W., 2002. Conodont apatite  $\delta^{18}\text{O}$  signatures indicate climatic cooling as a trigger  
685 of the Late Devonian mass extinction. Geology 30 (8) ,711–714.

686 Joachimski, M.M., von Bitter, P.H. and Buggisch, W., 2006. Constraints on Pennsylvanian glacioeustatic sea-level  
687 changes using oxygen isotopes of conodont apatite. Geology, 34(4): 277–280.

688 Joachimski, M. M., Pancost, R. D., Freeman, K. H., Ostertag-Henning, C., Buggisch, W., 2002. Carbon isotope  
689 geochemistry of the Frasnian–Famennian transition. Palaeogeography, Palaeoclimatology, Palaeoecology,  
690 181(1-3): 91–109.

691 Joachimski, M.M., Geldern, R.V., Breisig, S., Buggisch, W., Day, J., 2004. Oxygen isotope evolution of biogenic  
692 calcite and apatite during the Middle and Late devonian. International Journal of Earth Sciences  
693 (Geologische Rundschau) 93, 542–553.

694 Joachimski, M.M., Breisig, S., Buggisch, W., Talent, J.A., Mawson, R., Gereke, M., Morrow, J.R., Day, J., Weddige,  
695 K., 2009. Devonian climate and reef evolution: Insights from oxygen isotopes in apatite. Earth and  
696 Planetary Science Letters 284(3-4), 599–609.

697 Joachimski, M.M. and Lambert, L.L., 2015. Salinity contrast in the US Midcontinent Sea during Pennsylvanian  
698 glacio-eustatic highstands: Evidence from conodont apatite  $\delta^{18}\text{O}$ . Palaeogeography, Palaeoclimatology,  
699 Palaeoecology, 433: 71–80.

700 Johnson, J. G., Klapper, G., Sandberg, C. A., 1985. Devonian eustatic fluctuations in Euramerica. Geological Society  
701 of America, 96(5), 567–587.

702 Judd, E. J., Bhattacharya, T. and Ivany, L.C., 2020. A Dynamical Framework for Interpreting Ancient Sea Surface  
703 Temperatures. Geophysical Research Letters, 47(15): e2020GL089044.

704 Kennedy, K. L., Gibling, M. R., Eble, C. F., Gastaldo, R. A., Gensel, P. G., Werner-Zwanziger, U., Wilson, R. A.,  
705 2013. Lower Devonian coaly shales of northern New Brunswick, Canada: plant accumulations in the early  
706 stages of Terrestrial colonization. Journal of Sedimentary Research 83(12) , 1202–1215.

707 Krause, A. J., Mills, B. J. W., Zhang, S., Planavsky, N. J., Lenton, T. M. and Poulton, S. W. 2018. Stepwise  
708 oxygenation of the Paleozoic atmosphere. Nature communications 9, 4081.

709 Kravchinsky, V. A., 2012. Paleozoic large igneous provinces of Northern Eurasia: Correlation with mass extinction  
710 events. Global and Planetary Change 86–87, 31–36.

711 Kuszniir, N.J., Kovkhuto, A., Stephenson, R. A., 1996. Syn-rift evolution of the Pripyat Trough: constraints from  
712 structural and stratigraphic modeling. Tectonophysics 268, 221–236.

713 Lécuyer, C., Amiot, R., Touzeau, A., Trotter, J., 2013. Calibration of the phosphate  $\delta^{18}\text{O}$  thermometer with  
714 carbonate–water oxygen isotope fractionation equations. Chemical Geology 347(0), 217–226.

715 Le Hir, G., Donnadiou, Y., Goddérís, Y., Meyer-Berthaud, B., Ramstein, G., Blakey, R. C., 2011. The climate change

716 caused by the land plant invasion in the Devonian. *Earth and Planetary Science Letters* 310(3), 203–212.

717 Lenton, T. M., Dahl, T. W., Daines, S. J., Mills, B. J. W., Ozaki, K., Saltzman, M. R., Porada, P., 2016. Earliest land

718 plants created modern levels of atmospheric oxygen. *Proceedings of the National Academy of Sciences*

719 113(35), 9704–9709.

720 Lenton, T. M., Daines, S. J., Mills, B. J. W., 2018. COPSE reloaded: An improved model of biogeochemical cycling

721 over Phanerozoic time. *Earth Science Reviews* 178, 1–28.

722 Li, H., Ma, X. P., Wei, L. M., 2009. A new Middle–Upper Devonian boundary section in the open platform-platform

723 margin facies of Guilin, South China. *Acta Geologica Sinica* 83, 524–534.

724 Lipp, A.G., Shorttle, O., Sperling, E.A., Brocks, J.J., Cole, D.B., Crockford, P.W., Del Mouro, L., Dewing, K.,

725 Dornbos, S.Q., Emmings, J.F., Farrell, U.C., Jarrett, A., Johnson, B.W., Kabanov, P., Keller, C.B.,

726 Kunzmann, M., Miller, A.J., Mills, N.T., O’Connell, B., Peters, S.E., Planavsky, N.J., Ritzer, S.R.,

727 Schoepfer, S.D., Wilby, P.R., Yang, J. 2021. The composition and weathering of the continents over

728 geologic time. *Geochemical Perspectives Letter* 17, 21–26.

729 Liu, B. J., Xu, X. S., Pan, S. N., Huang, H. C., 1993. *Sedimentary-Crustal Evolution and Mineralization of the Paleo-*

730 *continent of South China*. Science Press, Beijing, 236 pp.

731 Lu, W., Ridgwell, A., Thomas, E., Hardisty, D.S., Luo, G., Algeo, T.J., Saltzman, M.R., Gill, B.C., Shen, Y., Ling,

732 H.-F., Edwards, C.T., Whalen, M.T., Zhou, X., Gutches, K.M., Jin, L., Rickaby, R.E.M., Jenkyns, H.C.,

733 Lyons, T.W., Lenton, T.M., Kump, L.R. and Lu, Z., 2018. Late inception of a resiliently oxygenated upper

734 ocean. *Science*, 361(6398): 174–177.

735 Ma, X. P., Wang, H. H., Zhang, M. Q., 2017. Devonian Event Succession and Sea Level Change in South China—

736 With Early and Middle Devonian carbon and oxygen isotopic data. *Subcommission on Devonian*

737 *Stratigraphy*, Newsletter 32:17–24.

738 Ma, X. P., Wang, C. Y., Racki, G., Racka, M., 2008. Facies and geochemistry across the Early–Middle Frasnian

739 transition (Late Devonian) on South China carbonate shelf: comparison with the Polish reference

740 succession. *Palaeogeography, Palaeoclimatology, Palaeoecology* 269, 130–151.

741 Ma, X. P., Liao, W. H., Wang, D. M., 2009. *The Devonian System of China, with a Discussion on Sea-Level Change*

742 *in South China*. Geological Society, London 314, 241–262.

743 Macarewicz, S.I., Poulsen, C.J. and Montañez, I.P., 2021. Simulation of oxygen isotopes and circulation in a late

744 Carboniferous epicontinental sea with implications for proxy records. *Earth and Planetary Science Letters*,

745 559: 116770.

746 Macdonald, F.A., Swanson-Hysell, N.L., Park, Y., Lisiecki, L., Jagoutz, O., 2019. Arc-continent collisions in the

747 tropics set Earth’s climate state. *Science* 364 (6436), 181–184.

748 Maher, K. and Chamberlain, C. P., 2014. Hydrologic Regulation of Chemical Weathering and the Geologic Carbon

749 Cycle. *Science* 343(6178), 1502–1504.

750 Matsunaga, K. K. S. and Tomescu, A. M. F., 2016. Root evolution at the base of the lycophyte clade: insights from

751 an Early Devonian lycophyte. *Annals of Botany* 117(4), 585–598.

752 McKenzie, N. R., Horton, B. K., Loomis, S. E., Stockli, D. F., Planavsky, N. J., Lee, C. T. A., 2016. Continental arc

753 volcanism as the principal driver of icehouse-greenhouse variability. *Science* 352(6284) , 444–447.

754 McMahon, W. J. and Davies, N. S., 2018. Evolution of alluvial mudrock forced by early land plants. *Science*

755 359(6379), 1022–1024.

756 Meyer-Berthaud, B., Scheckler, S. E., Wendt, J., 1999. *Archaeopteris* is the earliest known modern tree. *Nature*

757 398(6729), 700–701.

758 Meyer-Berthaud, B., Scheckler, S., Bousquet, J., 2000. The Development of *Archaeopteris*: New Evolutionary

759 Characters from the Structural Analysis of an Early Famennian Trunk from Southeast Morocco. *American*



760 journal of botany 87, 456–68.

761 Meyer-Berthaud, B., Soria, A., Decombeix, A. L., 2010. The land plant cover in the Devonian: a reassessment of the  
762 evolution of the tree habit. In: Vecoli, M., Clément, G., Meyer-Berthaud, B. (Eds.), *The Terrestrialization*  
763 *Process: Modelling Complex Interactions at the Biosphere–Geosphere Interface*. 339. Geological Society,  
764 Special Publications, London, pp. 59–70.

765 Mills, B. J. W., Scotese, C. R., Walding, N. G., Shields, G. A., Lenton, T.M., 2017. Elevated CO<sub>2</sub> degassing rates  
766 prevented the return of Snowball Earth during the Phanerozoic. *Nature Communications* 8(1), 1110.

767 Mills, B. J. W., Batterman, S. A. and Field, K. J., 2018. Nutrient acquisition by symbiotic fungi governs Palaeozoic  
768 climate transition. *Philosophical Transactions of the Royal Society B: Biological Science* 373,

769 Mills, B. J. W., Krause, A. J., Scotese, C. R., Hill, D. J., Shields, G. A., Lenton, T.M., 2019. Modelling the long-term  
770 carbon cycle, atmospheric CO<sub>2</sub>, and Earth surface temperature from late Neoproterozoic to present day.  
771 *Gondwana Research* 67, 172–186.

772 Mintz, J. S., Driese, S. G., White, J. D., 2010. Environmental and ecological variability of Middle Devonian  
773 (Givetian) forests in Appalachian Basin paleosols, New York, United States. *Palaios* 25, 85–96.

774 Mosbrugger, V., 1990. The tree habit in land plant. In: *Lecture Notes on Earth Sciences*. 28 Springer-Verlag, Berlin.

775 Morris, J. L., Richardson, J. B., Edwards, D., 2011. Lower Devonian plant and spore assemblages from the Lower  
776 Old Red Sandstone strata at Tredomen Quarry, SouthWales. *Review of Palaeobotany and Palynology* 165,  
777 183–208.

778 Morris, J. L., Leake, J. R., Stein, W. E., Berry, C. M., Marshall, J. E. A., Wellman, C. H., Milton, J. A., Hillier, S.,  
779 Mannolini, F., Quirk, J., Beerling, D. J., 2015. Investigating Devonian trees as geo-engineers of past  
780 climates: linking palaeosols to palaeobotany and experimental geobiology. *Palaeontology* 58(5) , 787–801.

781 Nelsen, M.P., DiMichele, W.A., Peters, S.E. and Boyce, C.K., 2016. Delayed fungal evolution did not cause the  
782 Paleozoic peak in coal production. *Proceedings of the National Academy of Sciences*, 113(9): 2442–2447.

783 Nöth, S., 1998. Conodont color (CAI) versus microcrystalline and textural changes in upper Triassic conodonts from  
784 northwest Germany. *Facies* 38, 165–173.

785 Pagani, M., Zachos, J. C., Freeman, K. H., Tiplle, B., Bohaty, S., 2005. Marked Decline in Atmospheric Carbon  
786 Dioxide Concentrations During the Paleogene. *Science*309(5734), 600–603.

787 Park, Y., Swanson-Hysell, N.L., Lisiecki, L.E., Macdonald, F.A., 2021. Evaluating the Relationship Between the  
788 Area and Latitude of Large Igneous Provinces and Earth's Long-Term Climate State. In: Ernst, R.E.  
789 Dickson A.J. and Bekker A. (Eds.), *Large Igneous Provinces*.

790 Prestianni, C., Gerrienne, P., 2010. Early seed plant radiation: an ecological hypothesis. In: Vecoli, M., Clément, G.,  
791 Meyer-Berthaud, B. (Eds.), *The Terrestrialisation Process: Modelling Complex Interactions at the*  
792 *Biosphere–Geosphere Interface*. Geological Society, London, Special Publications 339, pp. 71–80

793 Pucéat, E., Reynard, B., Lécuyer, C., 2004. Can crystallinity be used to determine the degree of chemical alteration  
794 of biogenic apatites? *Chemical Geology*, 205(1-2), 83–97.

795 Quirk, J., Andrews, M.Y., Leake, J. R., Banwart, S. A., Beerling, D. J., 2014. Ectomycorrhizal fungi and past high  
796 CO<sub>2</sub> atmospheres enhance mineral weathering through increased below-ground carbon-energy fluxes.  
797 *Biology letters* 10(7), 20140375.

798 Qie, W., Algeo, T. J., Luo, G., Herrmann, A., 2019. Global events of the Late Paleo-zoic (Early Devonian to Middle  
799 Permian): a review. *Palaeogeography, Palaeoclimatology, Palaeoecology* 531, 109259.

800 Qiao, L., Chen B., Shen, S. Z., 2021. Lower Devonian (Pragian) brachiopods from the Dashatian Section, Guangxi,  
801 South China. *Rivista Italiana di Paleontologia e Stratigrafia* 127(1), 1–16.

802 Racki, G., 2020. A volcanic scenario for the Frasnian–Famennian major biotic crisis and other Late Devonian global  
803 changes: More answers than questions? *Global and Planetary Change* 189, 103174

804 Raven, J. A. and Edwards, D., 2001. Roots: evolutionary origins and biogeochemical significance. *Journal of*  
805 *Experimental Botany* 52, 381–401.

806 Remy, W., Taylor, T.N., Hass, H., Kerp, H., 1994. Four hundred-million-year-old vesicular arbuscular mycorrhizae.  
807 *Proceedings of the National Academy of Sciences* 91, 11841–11843.

808 Rejebian, V.A., Harris, A.G., Huebner, J.S., 1987. Conodont colour and textural alteration: an index to  
809 regional metamorphism, contact metamorphism and hydrothermal alteration. *Geological Society of*  
810 *America Bulletin* 99, 471–497.

811 Rowe, N. and Speck, T., 2005. Plant growth forms: an ecological and evolutionary perspective. *New Phytologist*  
812 166(1), 61–72.

813 Rosenau, N. A., Tabor, N. J., Herrmann, A. D., 2014. Assessing the paleoenvironmental significance of middle-late  
814 Pennsylvanian conodont apatite  $\delta^{18}\text{O}$  values in the Illinois Basin. *Palaios* 29, 250–265.

815 Royer, D. L., Berner, R. A., Montañez, I. P., Tabor, N. J., Beerling, D. J., 2004. CO<sub>2</sub> as a primary driver of Phanerozoic  
816 climate. *GAS Today* 14(3), 4–10.

817 Royer, D. L., Donnadiou, Y., Park, J., Kowalczyk, J., Godd ris, Y., 2014. Error analysis of CO<sub>2</sub> and O<sub>2</sub> estimates  
818 from the long-term geochemical model GEOCARBSULF. *American Journal of Science* 314(9), 1259–  
819 1283.

820 Sandberg, C. A., Zigeler, W., Dreesen, R., Butler, J. L., 1988. Late Frasnian mass extinction: conodont event  
821 stratigraphy, global changes, and possible causes. *Courier Forschungsinstitut Senckenberg* 102, 263–307.

822 Savin, M. S., 1977. The history of the earth's surface temperature during the past 100 million years. *Annual review*  
823 *of earth and planetary sciences* 5, 319–355.

824 Simon, L., Godd is, Y., Werner, B., Strauss, H., Joachimski, M. M., 2007. Modeling the carbon and sulfur isotope  
825 compositions of marine sediments: Climate evolution during the Devonian. *Chemical Geology* 246(1–2),  
826 19–38.

827 Schopka, H. H., Derry, L. A., Arcilla, C. A., 2011. Chemical weathering, river geochemistry and atmospheric carbon  
828 fluxes from volcanic and ultramafic regions on Luzon Island, the Philippines. *Geochimica et*  
829 *Cosmochimica Acta* 75(4), 978–1002.

830 Schmidt, G. A., Bigg, G. R., Rohling, E. J., 1999. Global seawater oxygen-18 database. [http:// data.giss.nasa.gov.o18](http://data.giss.nasa.gov/o18)  
831 [data](http://data.giss.nasa.gov/o18).

832 Stein, W. E., Mannolini, F., Hernick, L. V., Landing, E., Berry, C. M., 2007. Giant cladoxylopsid trees resolve the  
833 enigma of the Earth's earliest forest stumps at Gilboa. *Nature* 446, 904–907.

834 Stein, W. E., Berry, C. M., Hernick, L. V., Mannolini, F., 2012. Surprisingly complex community discovered in the  
835 mid-Devonian fossil forest at Gilboa. *Nature* 483, 78–81.

836 Stewart, E. M. and Ague, J. J., 2018. Infiltration-driven metamorphism, New England, USA: Regional CO<sub>2</sub> fluxes  
837 and implications for Devonian climate and extinctions. *Earth and Planetary Science Letters* 489, 123–134.

838 Streel, M., Caputo, M.V., Loboziak, S., Melo, J. H. G., 2000. Late Frasnian–Famennian climates based on  
839 palynomorph analyses and the question of the Late Devonian glaciations. *Earth Science Reviews* 52, 121–  
840 173.

841 Strullu–Derrien, C., Kenrick, P., Pressel, S., Duckett, J. G., Rioult, J. P., Strullu, D. G., 2014. Fungal associations in  
842 *Horneophyton ligneri* from the Rhynie Chert (c. 407 Ma) closely resemble those in extant lower land plants:  
843 novel insights into ancestral plant–fungus symbioses. *New Phytologist* 203, 964–979.

844 Shen, S.Z., Ramezani, J., Chen, J., Cao, C., Erwin, D., Zhang, H., Xiang, L., Schoepfer, S., Henderson, C., Zheng,  
845 Q., Bowring, S., Wang, Y., Li, X. H., Wang, X.D., Yuan, D., Zhang, Y., Lin, M., Wang, J., Wu, Y.S.,  
846 2019. A sudden end-Permian mass extinction in South China. *GSA Bulletin* 131, 205–223.

847 Shen, Z., Monnet, C., Cascales-Mi ana, B., Gong, Y., Dong, X., Kroeck, D. M., Servais, T., 2020. Diversity

848 dynamics of Devonian terrestrial palynofloras from China: Regional and global significance. *Earth Science*  
849 *Reviews*, 200, 102967.

850 Tao, K., Robbins, J.A., Grossman, E.L., O’Dea, A., 2013. Quantifying upwelling and freshening in nearshore tropical  
851 American environments using stable isotopes in modern gastropods. *Bulletin Marine Science*. 89, 815–  
852 835.

853 Taylor, T. N., Taylor, E. L., Krings, M., 2009. *Paleobotany: The Biology and Evolution of Fossil Plants*, second  
854 edition. Academic Press, Amsterdam.

855 Tostevin, R. and Mills, B. J. W., 2020. Reconciling proxy records and models of Earth's oxygenation during the  
856 Neoproterozoic and Palaeozoic. *Interface Focus* 10 4 20190137

857 Trotter, J.A., Williams, I.S., Nicora, A., Mazza, M. and Rigo, M., 2015. Long-term cycles of Triassic climate change:  
858 a new  $\delta^{18}\text{O}$  record from conodont apatite. *Earth and Planetary Science Letters*, 415: 165–174. Valdes, P.  
859 J., Scotese, C. R., and Lunt, D. J. 2021. Deep ocean temperatures through time, *Climate of the Past*, 17,  
860 1483–1506.

861 Van Der Meer, D. G., Zeebe, R. E., van Hinsbergen, D. J. J., Sluijs, A., Spakman, W., Torsvik, T. H., 2014. Plate  
862 tectonic controls on atmospheric CO<sub>2</sub> levels since the Triassic. *Proceedings of the National Academy of*  
863 *Sciences* 111(12), 4380–4385.

864 Van Geldern, R., Joachimski, M. M., Day, J., Jansen, U., Alvarez, F., Yolkin, E. A., Ma, X. P., 2006. Carbon, oxygen  
865 and strontium isotope records of Devonian brachiopod shell calcite. *Palaeogeography, Palaeoclimatology,*  
866 *Palaeoecology* 240(1–2), 47–67.

867 Volk, T., 1987. Feedbacks between weathering and atmospheric CO<sub>2</sub> over the last 100 million years. *American Journal*  
868 *of Science* 287, 763–779

869 Wang, C. Y., 1994. Application of the Frasnian standard conodont zonation in South China. *Courier*  
870 *Forschungsinstitut Senckenberg* 168, 83–129.

871 Wang, C. Y., Ziegler, W., 2002. The Frasnian–Famennian conodont mass extinction and recovery in South China.  
872 *Senckenb. Lethaea* 82, 463–493.

873 Wang, C. Y., Wang, P., Yang, G. H., Xie, W., 2009. The restudy of Silurian Conodont biostratigraphy in the Baizitian  
874 Section in Yanbian, Sichuan. *Journal of Stratigraphy* 33 (3), 302–317.

875 Wang, C.Y., Chen, B., Kuang G. D., 2016 Lower Devonian conodonts from the Nagaoling Formation of the  
876 Dashatian section near Nanning, Guangxi, South China. *Acta Micropalaeontologica Sinica* 33(4), 420–  
877 435.

878 Wang, Y., Wang, J., Xu, H. H., He, X. Z., 2010. The evolution of Paleozoic vascular land plant diversity of South  
879 China. *China Earth Science* 53, 1828–1835.

880 Wang, D. M. and Lin, Y. J., 2007. A New Species of Metacaladophyton from the Late Devonian of China. *International*  
881 *Journal of Plant Sciences* 168 (7), 1067–1084.

882 Wang, D. M. and Liu, L., 2015. A new Late Devonian genus with seed plant affinities. *BMC Evolutionary Biology*  
883 15, 28.

884 Wehrmann, A., Hertweck, Günther., Brocke, Rainer., Jansen U., Königshof, P., Plodowski, G., Schindler E., Wilde,  
885 V., Blicke, A., Schultka., S., 2005. Palaeoenvironment and palaeoecology of intertidal deposits in a Lower  
886 Devonian siliciclastic sequence of the Mosel Region, Germany. *Palaios* (20), 101–120.

887 Wilson, M., Lyashkevich, Z. M., 1996. Magmatism and the geodynamics of rifting of the Pripyat–Dnieper–Donets  
888 rift, East European Platform. *Tectonophysics* 268, 65–81.

889 Wu, Y., Zhou, H. L., Jiang T. C., Fang D. N., Huang, S. W., 1987. *Sedimentary Facies Paleogeography and relatively*  
890 *Mineral Deposits of Devonian in Guangxi*. People’s Publishing House of Guangxi, Nanning, 1–292.

891 Xue, J., Huang, P., Ruta, M., Benton, M. J., Hao, S. G., Xiong, C. H., Wang, D. M., Cascales-Miñana, B., Wang, Q.,

892 Liu, L., 2015. Stepwise evolution of Paleozoic tracheophytes from South China: contrasting leaf disparity  
893 and taxic diversity. *Earth Science Reviews* 148, 77–93.

894 Xue, J., Deng, Z., Huang, P., Huang, K., Benton, M. J., Cui, Y., Wang, D., Liu, J., Shen, B., Basinger, J. F., Hao, S.,  
895 2016. Belowground rhizomes in paleosols: The hidden half of an Early Devonian vascular plant.  
896 *Proceedings of the National Academy of Sciences* 113(34), 9451–9456.

897 Xue, J., Huang, P., Wang, D., Xiong, C., Liu, L., Basinger, J. F., 2018. Silurian–Devonian terrestrial revolution in  
898 South China: Taxonomy, diversity, and character evolution of vascular plants in a paleogeographically  
899 isolated, low latitude region. *Earth Science Reviews*, 180, 92–125.

900 Zazzo, A., Lécuyer, C. and Mariotti, A., 2004. Experimentally-controlled carbon and oxygen isotope exchange  
901 between bioapatites and water under inorganic and microbially-mediated conditions. *Geochimica et*  
902 *Cosmochimica Acta*, 68(1): 1–12.

903 Ziegler, W. and Wang, C. Y., 1985. Sihongshan section, a regional reference section for the Lower–Middle and  
904 Middle–Upper Boundaries in Far East Asia. *Courier Forschungsinstitut Senckenberg* 75, 17–38.

918

919

920

921

922

923

924

925

926

927

928

929

930

931

932

933

934

935

936

937

938

939

940

941

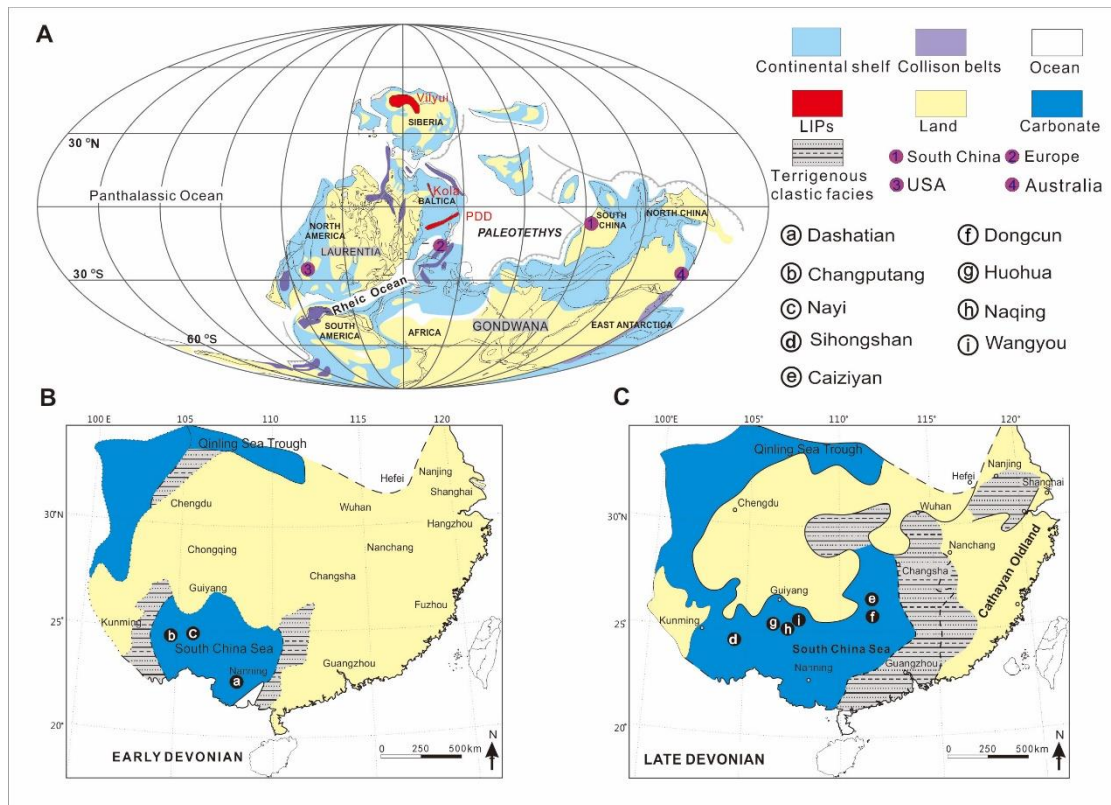
942

943

944

945

946



947

948

949 Fig. 1. A: Global palaeogeographic reconstruction for the Middle/Late Devonian

950 (revised from Golonka, 2000). B and C: Early and Late Devonian palaeogeographic

951 reconstructions for South China and location of study sections (revised from Ma et al.,

952 2009).

953

954

955

956

957

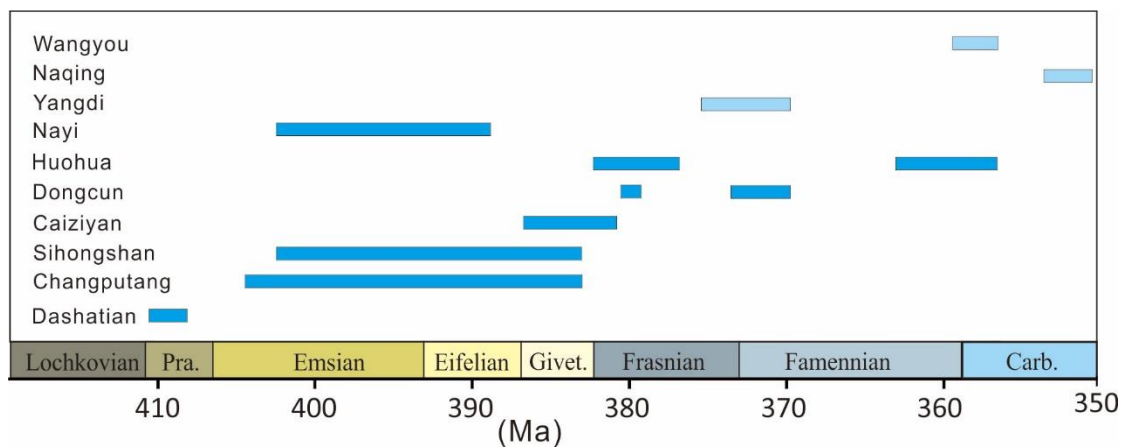
958

959

960

961

962



963

964 Fig. 2. Stratigraphic range of sections studied in South China. Absolute ages after  
 965 Geological Timescale 2012 (Gradstein et al., 2012). Light blue box represents sections  
 966 reported in Huang et al., 2018 and Chen et al., 2021. Pra. = Pragian, Givet. = Givetian,  
 967 Carb. = Carboniferous

968

969

970

971

972

973

974

975

976

977

978

979

980

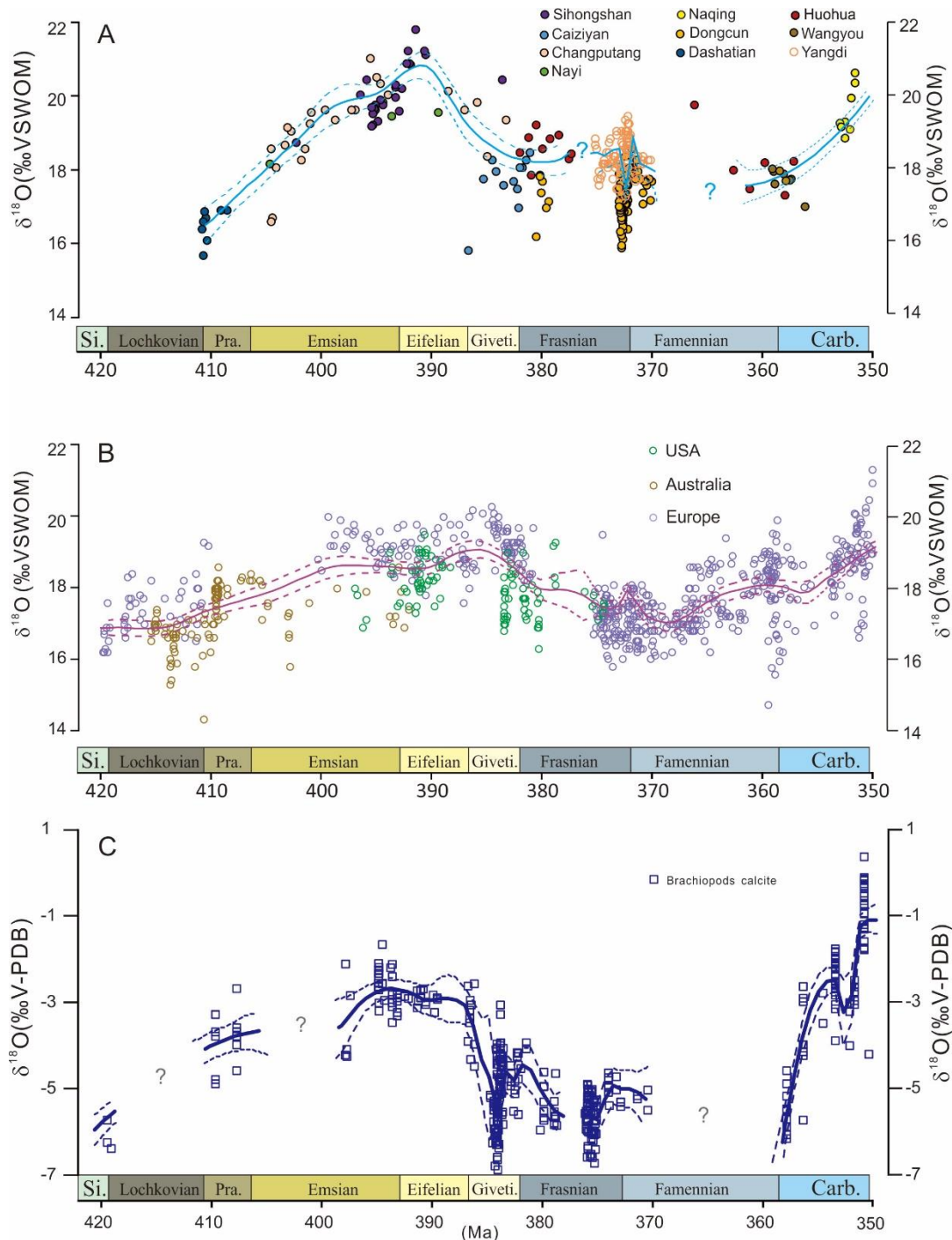
981

982

983

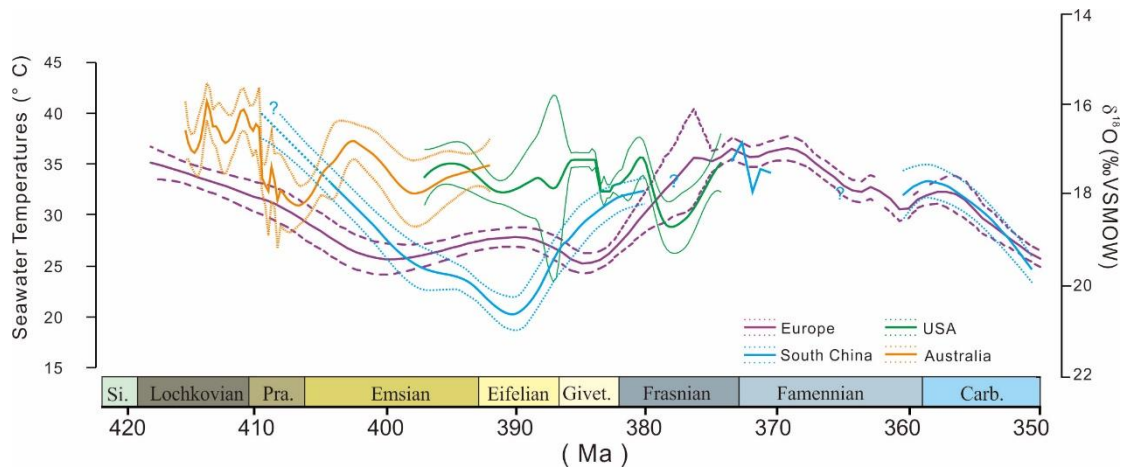
984

985



987

988 Fig. 3. South China conodont apatite  $\delta^{18}\text{O}$  record (A) compared with published  
 989  $\delta^{18}\text{O}_{\text{apatite}}$  (B) (Joachimski et al., 2009; Elrick et al., 2009; Girard et al., 2020) and  
 990 brachiopod  $\delta^{18}\text{O}_{\text{calcite}}$  records (C) (van Geldern et al., 2006). Solid lines represent Locfit  
 991 regression, dotted lines give 95% confidence interval. All published data are  
 992 recalibrated to Geological Timescale 2012 (Gradstein et al., 2012). Si = Silurian, Pra.  
 993 = Pragian, Givet. = Givetian, Carb. = Carboniferous



994

995 Fig. 4. Comparison of Devonian temperature records from different paleocontinents.

996 Solid lines give Locfit regressions for samples from South China (data from the

997 Dashatian section is excluded since  $\delta^{18}\text{O}$  likely influenced by freshwater input), Europe,

998 USA and Australia; dotted lines give 95% confidence interval. Temperature calculated

999 using temperature equations given by [Lécuyer et al. \(2013\)](#) assuming an average

1000 oxygen isotope value for Devonian oceans of  $-1\text{‰ VSMOW}$ . Abbreviations as Fig. 3

1001

1002

1003

1004

1005

1006

1007

1008

1009

1010

1011

1012

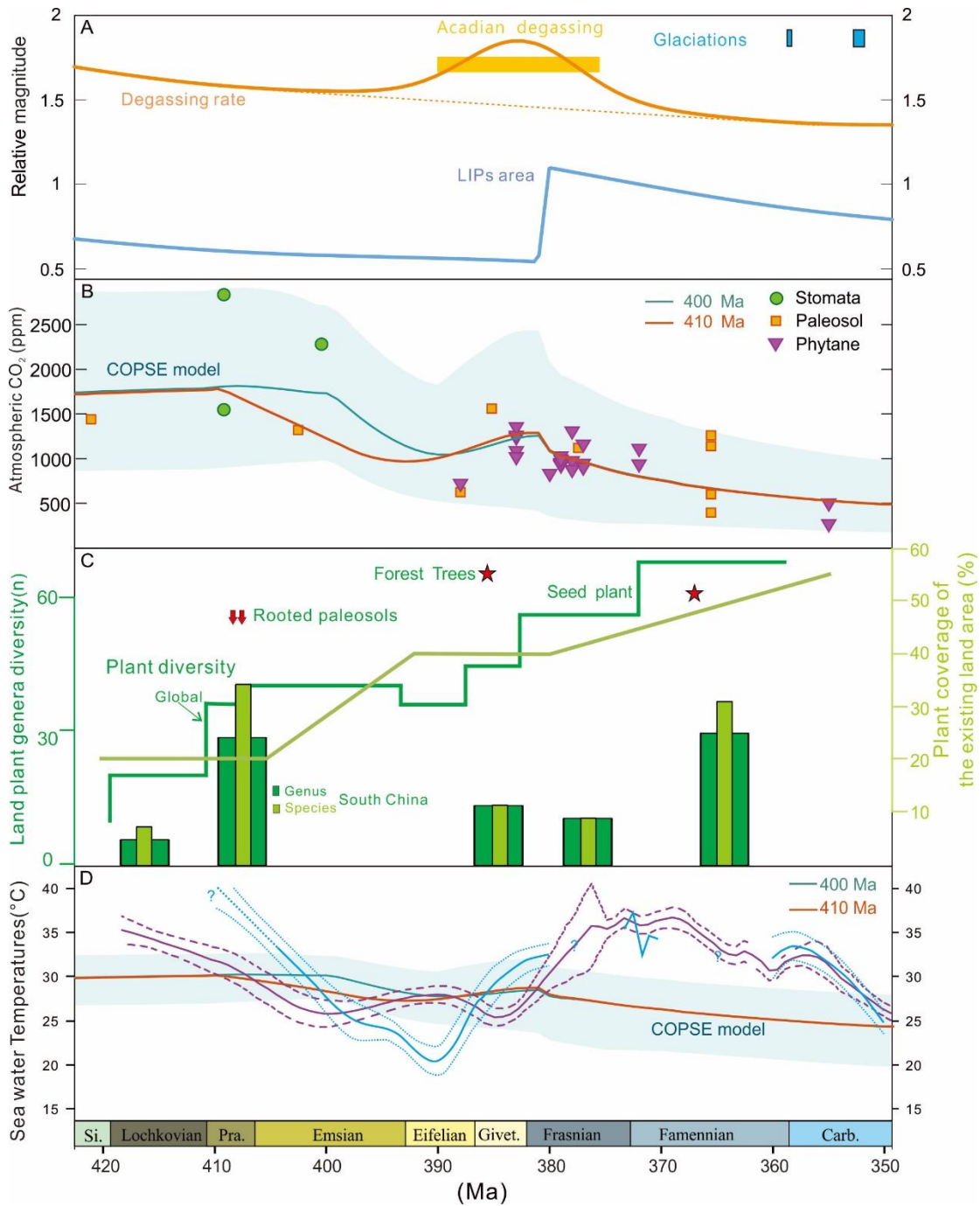
1013

1014

1015

1016





1017

1018 Fig. 5. Comparison of Devonian temperature records with significant events in  
 1019 terrestrial vascular plants,  $p\text{CO}_2$ , volcanism and glaciation records. (A) Global LIPs  
 1020 (and other mafic rock) area and tectonic  $\text{CO}_2$  degassing rate (magnitude normalized to  
 1021 the present) used to compute the COPSE model (Mills et al., 2017; 2019), including  
 1022 degassing pulse due to Acadian orogenic activity (Stewart and Ague, 2018), and  
 1023 glaciation record (Caputo et al., 2008). (B) Proxy (Royer et al., 2014; Foster et al.,  
 1024 2017) and modelling (Lenton et al., 2018; Tostevin and Mills, 2020) reconstructions  
 1025 of atmospheric  $p\text{CO}_2$  by assuming significant radiation of rooted terrestrial vegetation

1026 started at ~410 or ~400 Ma. (C) Significant plants innovation events (Red Arrow and  
1027 Pentacle, [Stein et al., 2012](#); [Matsunaga and Tomescu, 2016](#); [Xue et al., 2016](#)), mega  
1028 plant fossil diversities (Green line, Global Plant fossil diversity, [Cascales-Minana,](#)  
1029 [2016](#); and Histogram, Genus and Species level fossil diversity from South China, [Xue](#)  
1030 [et al., 2018](#)) and terrestrial plant coverage in the existing land (Light green line, [Simon](#)  
1031 [et al., 2006](#)) (D) Devonian low latitude temperature records (as Fig. 3) compared to  
1032 low latitude temperatures modelled by COPSE. Abbreviations as Fig. 3.

1033

1034

1035

1036

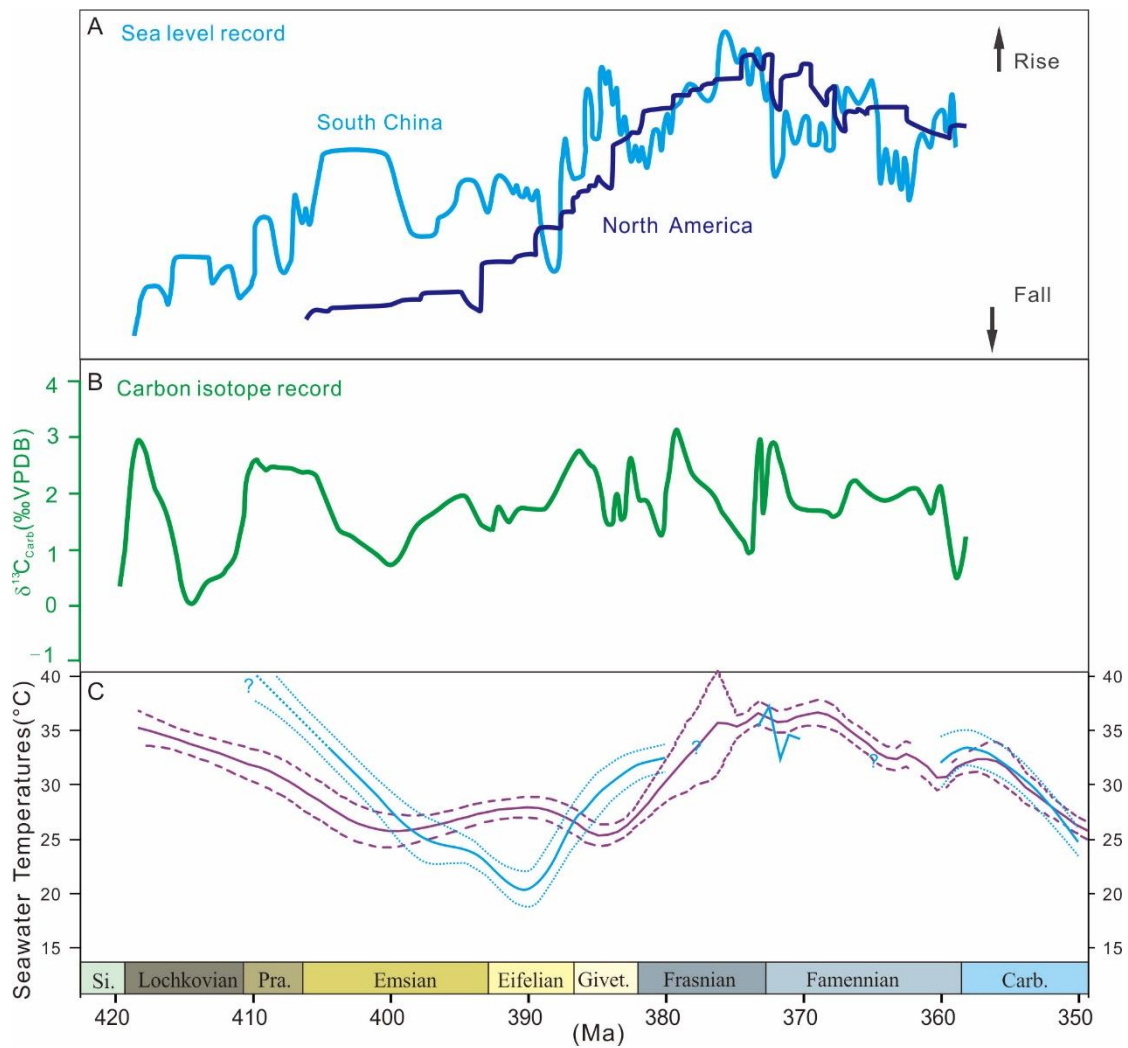
1037

1038

1039

1040

1041



1042

1043 Fig. 6. Comparison of Devonian temperature records with sea level changes and

1044 carbonate  $\delta^{13}\text{C}_{\text{carb}}$  record. (A). North America (Johnson et al., 1985) and South China

1045 (Ma et al., 2009) relative sea level change curves (B)  $\delta^{13}\text{C}_{\text{carb}}$  record from whole rock

1046 carbonate (Buggisch and Joachimski, 2006), (C) Devonian temperature records (this

1047 study). Abbreviations as Fig. 3.